SANDIA REPORT
SAND2015-10224
Unlimited Release
Printed November 2015

On Radar Resolution in Coherent Change Detection

Douglas L. Bickel

Prepared by
Sandia National Laboratories
Albuquerque, New Mexico 87185 and Livermore, California 94550

Sandia National Laboratories is a multi-program laboratory managed and operated by Sandia Corporation, a wholly owned subsidiary of Lockheed Martin Corporation, for the U.S. Department of Energy's National Nuclear Security Administration under contract DE-AC04-94AL85000.

Issued by Sandia National Laboratories, operated for the United States Department of Energy by Sandia Corporation.

Available to DOE and DOE contractors from

U.S. Department of Energy
Office of Scientific and Technical Information
P.O. Box 62
Oak Ridge, TN 37831

Telephone: (865) 576-8401
Facsimile: (865) 576-5728
E-Mail: reports@adonis.osti.gov
Online ordering: http://www.osti.gov/bridge

Available to the public from

U.S. Department of Commerce
National Technical Information Service
5285 Port Royal Rd.
Springfield, VA 22161

Telephone: (800) 553-6847
Facsimile: (703) 605-6900
E-Mail: orders@ntis.fedworld.gov
Online order: http://www.ntis.gov/help/ordermethods.asp?loc=7-4-0#online

SAND2015-10224
Unclassified Unlimited Release
Printed November 2015

On Radar Resolution in Coherent Change Detection

Douglas L. Bickel
ISR Analysis and Application
Sandia National Laboratories
PO Box 5800
Albuquerque, NM 87185-0519

ABSTRACT

It is commonly observed that resolution plays a role in coherent change detection. Although this is the case, the relationship of the resolution in coherent change detection is not yet defined. In this document, we present an analytical method of evaluating this relationship using detection theory. Specifically we examine the effect of resolution on receiver operating characteristic curves for coherent change detection.

ACKNOWLEDGEMENTS

The preparation of this report is the result of an unfunded research and development activity.

Sandia National Laboratories is a multi-program laboratory managed and operated by Sandia Corporation, a wholly owned subsidiary of Lockheed Martin Corporation, for the U.S. Department of Energy's National Nuclear Security Administration under contract DE-AC04-94AL85000.

CONTENTS

This page left intentionally blank.

1. Executive Summary

This report gives a general model for radar designers to analyze coherent change detection performance with radar resolution. The analysis of the performance is based on receiver operating characteristic curves from detection theory. The model is developed for three different statistical cases of the size of the change region relative to the resolution. The first is when the change region is at least as large as the area covered by multilook estimation window used in coherence estimation. The second is where the change region is smaller than the multilook estimation window size, but larger than the synthetic aperture radar resolution size. The third is where the change region is smaller than the synthetic aperture radar resolution.

This page left intentionally blank.

2. Introduction

As with all radar imaging techniques, resolution is a critical quantity in coherent change detection (CCD). The problem is that in CCD we deal with complex scene content that is best described probabilistically. The result is that the simplicity of the Rayleigh resolution does not adequately describe the complexity of the effect of resolution in CCD. At its core, the CCD problem is a detection problem. In this document we discuss this problem from a probabilistic viewpoint where the Rayleigh radar resolution is an important input parameter. We will examine detection of changes as a function of the size of the change versus Rayleigh resolution by developing an analytical model to represent the process. We also point out that in CCD there are two different resolutions. The first is the familiar synthetic aperture radar (SAR) imaging Rayleigh resolution. The second is a "spoiling" of the resolution by the multilook operation used for coherence estimation in CCD. Both quantities play a role in model developed for detection.

In this document we present a mathematical framework for comparing different resolutions in terms of CCD performance. In general, this is a difficult subject. Although the math in this document is complicated, the model itself has been simplified. The result is a basic framework to discuss resolution in CCD within the limitations of the model. It is postulated that this model represents a baseline analysis

The unique contribution of this document is to extend the current analysis of CCD detection to smaller regions of change than considered in [PREI06] and [BICK15]. Both of these hint at the issues addressed in this document. In general, this extension is mathematically difficult. In this document we take advantage of a known (but not generally well-known) statistical approximation to extend the analysis to incorporate a more general case. As in [PREI06] and [BICK15], we base this analysis on considering this a detection problem.

It is important to indicate that we are considering the effects of resolution in CCD aside from any other issues. In other words, we assume consistency in processing, registration, etc. In addition, even though resolution can affect the signal-to-noise ratio (SNR), we will do not directly address this issue in this document; rather, we provide the reader to tools to perform this trade-off[1].

In section 3, we discuss resolution as pertains to CCD and introduce a model of resolution where we partition the analysis into three separate cases. In section 4 we apply this model to the CCD detection problem. In section 5 we briefly present a possible slight adjustment to the analytical model. In section 6 we examine the implications from the model and the limitations of the model. In section 7 we discuss other considerations for resolution and CCD that are outside the scope of the model presented in this document. In the final section, we give concluding remarks.

[1] More accurately, we assume that the SNR is incorporated in whatever background coherence we assume, and the background coherence will be a parameter in this report. This report provides the tools for a more in depth consideration.

In this document, it will be assumed that the reader is intimately familiar with coherent change detection in the context of synthetic aperture radar.

3. Resolution and CCD

Key concepts in this section: The size of the change regions relative to the resolution is an important parameter. There are two resolutions of interest for CCD which are the radar (Rayleigh) resolution, and the size ("resolution") of the multilook coherence estimation window. Therefore, the development is considered as three distinct cases of the size of the change region relative to these resolutions. They are: 1) the size of the region with change is larger than or equal to the size of the region used for multilook estimation of the coherence; 2) the size of the change region is less than the multilook resolution but at least the size of the radar resolution; or 3) the size of the change region is less than a radar resolution.

It is well-known that resolution is a key parameter in CCD. In spite of this fact, and the obvious qualitative improvement, there is currently no clear method of evaluating the effectiveness of improving the resolution on CCD performance.

In CCD we are attempting to identify a region of change by a examining a given region for a deviation in coherence relative to the coherence in the surrounding areas. As the "D" in CCD suggests, this is a detection problem. In general, due to the probabilistic nature of detection problems we want to have as much information as possible to make a confident decision. Finer radar resolution allows us to have more pixels on the change and no-change regions leading to a benefit in the decision process[2]. Intuitively, if possible, we would not want to mix the two regions in the detection decision. In other words ideally we would not want to mix change pixels with no-change pixels during coherence estimation[3]. Again, finer resolution permits us more fidelity in this separation.

In CCD, there are two resolutions of interest[4]. The first resolution is the one we typically think of, namely the standard SAR Rayleigh resolution. We will designate this resolution by the variable, ρ_R. The second is the resolution caused by the "multilook" operation in the coherence estimation process (see [BICK14] and references therein). This multilook process acts as a low-pass filter which can be thought of as a loss of resolution on the coherence product. We will refer to this by the variable, ρ_{ml}. In order to perform reasonable coherence estimation, we require $\rho_{ml} > \rho_R$. In fact in this document we will assume in this document that $\rho_{ml} = L\rho_R$, where L is an integer equal to the number of independent looks used in the coherence estimation. Figure 1 is repeated from Appendix A for convenience and illustrates the two resolutions.

[2] Provided all other considerations remain the same.
[3] In a philosophical sense, this is like Wiener filtering.
[4] Note that in our discussion of CCD, the resolution is really an area, i.e., a 2D resolution cell size.

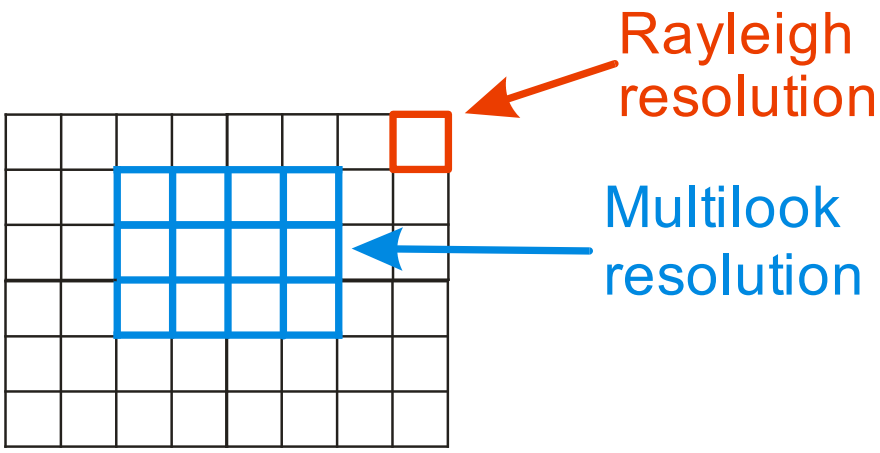

Figure 1: Illustration of two resolutions in CCD in terms of image pixels (in the illustration $\rho_{ml} = 12\rho_R$)

Based upon this preceding discussion we will define our model in this document in terms of three separate cases. We define the "size" of the change region as Γ_c [5]. The first region is for $\Gamma_c \geq \rho_{ml}$. The next region is for $\rho_{ml} > \Gamma_c \geq \rho_R$ subject to $\Gamma_c = k\rho_R \quad k \in$ positive integer [6]. The final region we will consider is $\Gamma_c < \rho_R$. The three cases are illustrated in Figure 2 below. In this figure, the black grid cells represent the SAR Rayleigh resolution cells. The light blue cells indicate the size of the multilook coherence estimation box size. The gray colored areas are the areas of change. The filled-in white areas are the no-change, or quiescent regions.

More discussion on the model is in Appendix A. The reason for the partitioning into these regions will be discussed in the following sections.

[5] In follow on discussion, we will note that we are interested in the change region normalized by the Rayleigh resolution, $\Gamma = \Gamma_c / \rho_R$.

[6] This integer assumption allows us to present the required analysis without adding complexity that creates unnecessary confusion. We note that the analysis presented in this document can be extended to the more general case, but becomes quite complicated.

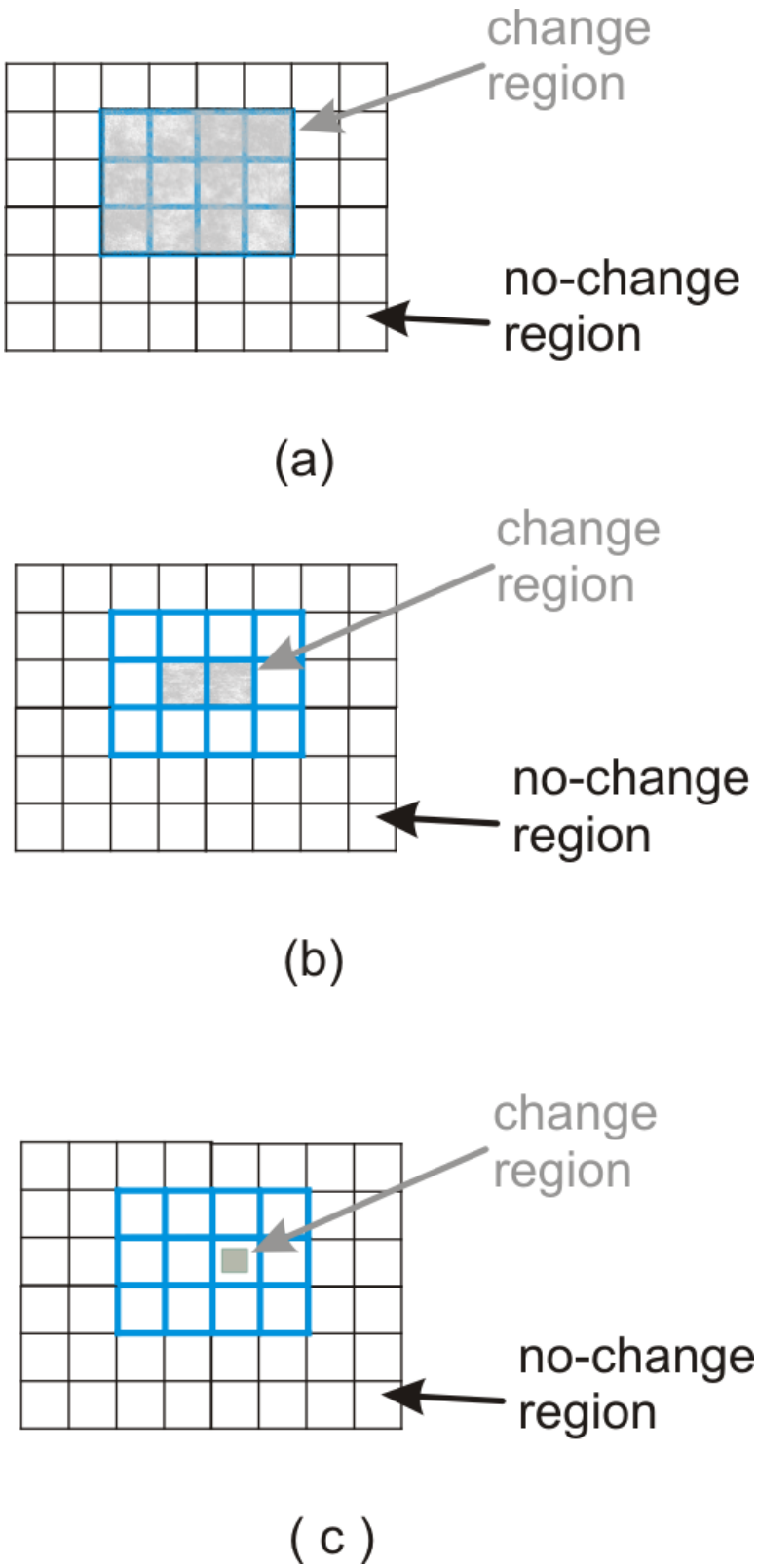

Figure 2: Three different change region cases (a) change covers an entire multilook resolution cell; (b) change covers a partial multilook resolution cell (c) change covers partial Rayeigh resolution cell

This page left intentionally blank.

4. Analytical model for resolution and CCD

Key concepts in this section: Coherent Change Detection (CCD) is about detection of change via unexpected change in the coherence between two images. The effect of resolution is analyzed from a detection theory viewpoint. This section shows that the three cases of change size from the previous section must be considered separately because the statistical behavior for each case is different. The mathematical model for each case is presented. We suggest that there is a benefit from normalizing all different resolutions and change regions relative to the size of the raw SAR resolution.

We now present an analytical model to describe the effect of resolution on CCD. In this section we discuss the proposed model and how it relates resolution to the CCD receiver operating characteristic (ROC) curve performance. The relevant math and detection theory for this analysis is developed in Appendix A, B and C. We will repeat some of the pertinent information from the appendices in the follow sections.

4.1 Overview

To briefly recap, it is our goal in this document to develop an analytical method to evaluate the effect that resolution has on the detection of change in CCD. In this document we derive an analytic model for the ROC curves to describe CCD detection as a function of the quiescent coherence and resolution. The ROC curves require the cumulative probability density functions that correspond to the hypotheses of interest. Effectively, the ROC curves describe the separation of the probabilities of the hypotheses of interest as a function of parameters. In our case, the hypotheses will be H_1 when a change has occurred, or H_0 when no-change has occurred within a specific region of attention. The main parameter that we wish to investigate is the radar resolution, although other parameters, such as quiescent coherence, and number of independent looks will play a significant role. Intuitively, the size of the region of change relative to the Rayleigh resolution cell size is key. Without loss of generality, we will assume the size of the change region is normalized relative to the size of a resolution cell.

We wish to analyze our success in selecting the appropriate hypothesis between change, H_1, and no-change, H_0. We will use the conventional Neyman-Pearson detection criteria [SHAN88] of a detection decision relative to a choice of threshold. Recalling that detection decision in CCD is the converse of what we typically find in radar, we will declare for H_1 if the estimated coherence is *less than* the choice of threshold. In other words, we declare that a change has occurred in a region if $\hat{\mu} < \lambda_{th}$, where $\hat{\mu}$ is the

estimated sample coherence[7] for the pixel and λ_{th} is the chosen threshold. Otherwise, we will declare for H_0, or no-change, if $\hat{\mu} > \lambda_{th}$ for that region within the CCD image.

Following traditional radar convention, we declare that the probability of detection, P_D, is the probability that we select H_1 when there is a coherence change present. The probability of detection is therefore given by:

$$P_D = P\left(\hat{\mu} \le \lambda_{th} \middle| \mu_c, \mu_q, L\right) \tag{1}$$

where μ_c is the population coherence of the change region we evaluate, μ_q is the quiescent (or surrounding no change) population coherence, and L the number of independent looks. Note that the region which we evaluate for change can be larger or smaller than the true region of change. In the true region of change we will assume that it has a population coherence of zero. The justification for this assumption follows from [ZEBK92] (and repeated in [PREI06]), which indicate that if the disturbance of the scatters results in an RMS "motion" of approximately 20% to 30% of a wavelength, we can assume total decorrelation.

The error hypothesis of interest will be the probability of choosing hypothesis H_1 when there is no change present, which is the probability of false-alarm, P_{FA}. The probability of a false-alarm is then given by:

$$P_{FA} = P\left(\hat{\mu} \le \lambda_{th} \middle| \mu_q, L\right) \tag{2}$$

where P_{FA} is the probability of false-alarm, and μ_q is the population coherence of the no-change (quiescent) region.

4.2 Model

This section discusses an analytical model of how resolution comes into play in CCD and uses this model to derive CCD performance as a function of resolution.

As in [PREIS06], we come at this from a detection theory point of view. The "target" signal that we wish to detect is *decorrelated* clutter and *decorrelated* noise between two SAR images, which we differentiate from a quiescent background of *correlated* clutter and *decorrelated* noise. All resolution cells are assumed to be independent. Following convention all clutter and noise will be assumed to be random variables drawn from

---

[7] In this document the estimate of the coherence is referred to as the sample coherence and is designated with the "hat" or circumflex symbol, e.g. $\hat{\mu}$. The true coherence that we are trying to estimate is referred to as the population coherence and has no "hat", e.g. μ.

complex circularly Gaussian distributions. The assumption is made in this document that the clutter decorrelation process does not affect the average clutter backscatter magnitude.

The detection problem in this analysis will be parameterized by SAR Rayleigh resolution and with the number of independent looks, L, used to estimate the coherence, as well as with the quiescent coherence. The multilook resolution is implicitly a function of the Rayleigh resolution and the number of looks. In fact as noted above, in this document we assume it is the product of these two parameters. The probability of detection versus false-alarm rate as a function of the parameters and the detection threshold will be represented by ROC curves.

The radar resolution comes into play in CCD by virtue of the fact that the number of resolution cells on the change region affects the coherence estimation performance. If the change region is large with respect to the resolution, then we can achieve the number of independent looks we wish to achieve for good coherence estimation. However, if the change region is relatively small with respect to the radar resolution, then the number of looks available in the change region is limited. The choice of the number of looks is used to improve the estimation of the coherence of the quiescent background. It sets the "multilook resolution". In CCD performance, if all else is equal, in theory finer multilook resolution allows for more independent looks for a given multilook resolution, which in turn leads to lower coherence variance. A trade-off occurs when radar resolution is coarse and we want a specific number of independent looks to achieve a low variance. Then the multilook resolution, or even the SAR resolution can become large with respect to the change region. For this case, the multilook operation leads to a dilution in the no-change region due to attempting to estimate change coherence with data that includes both change and no-change. Therefore, the no change region in our estimator is a mixture of change and no-change statistics. We will address detection performance for the mixed and non-mixed coherence estimation in this document. This will allow us to generalize the CCD performance with respect to resolution. Obviously from the above discussion it is the size of the change region *relative to radar resolution* that is important, taken aside from all other considerations[8]. Since this is the case, we repeat the above statement that without loss of generality we can consider all regions in this analysis normalized to the size of the SAR Rayleigh resolution.

The model in this document considers the following cases: 1) changes at least as large as the multilook resolution (window size) used for coherence estimation; 2) changes larger than a SAR resolution cell, but smaller than a multilook resolution cell; 3) changes smaller than a SAR resolution cell. The first will lead to no mixing. The second case will lead to one type of mixing, that we will describe below. The third case leads to a different type of mixing yet. Hence, the reason for considering the three cases separately is because of the difference in the type of mixing that occurs in each case leads to different statistical models.

[8] For example, assuming that the clutter-to-noise ratio is not affected by the change in resolution.

In the following subsections, we will present the results of the analytical model developed in the appendices for each of these resolution cases. Although we will only present the results of the analytical models, as noted in the appendices we want to point out that the key to the mathematical model developed in this document is that regardless of the resolution case we will approximate the sample covariance matrix as a complex central Wishart distribution.

4.3.1 Model with change region larger than multilook resolution[9]

This subsection discusses the model under the assumption that the change region is large with respect to the multilook resolution size. In this case, the probability density function (pdf) of the coherence function under the Gaussian assumptions is repeated from [TOUZ96]:

$$p\left(\hat{\mu}\middle|\mu,L\right)=2\left(L-1\right)\left(1-\mu^2\right)^L\,\hat{\mu}\left(1-\hat{\mu}^2\right)^{(L-2)}\,{}_2F_1\left(L,L;1;\hat{\mu}^2\mu^2\right) \tag{3}$$

with ${}_2F_1\left(a,b;c;d\right)$ being the Gauss hypergeometric function.

A *key assumption* in the equation above is that the population coherence is stationary across the entire L look cell used for coherence estimation, i.e., the multilook resolution cell[10]. Since we are limiting the model considered in this subsection to change and no-change regions that are larger than the multilook resolution size, therefore we implicitly meet this requirement by assumption.

The corresponding cumulative distribution from [CART73] for integer L is:

$$P\left(\hat{\mu}<\lambda_{th}\middle|\mu,L\right)=\lambda_{th}^2\left(\frac{1-\mu^2}{1-\mu^2\lambda_{th}^2}\right)^L\sum_{k=0}^{L-2}\left(\frac{1-\mu^2}{1-\mu^2\lambda_{th}^2}\right)^k\,{}_2F_1\left(-k,1-L;1;\mu^2\lambda_{th}^2\right) \tag{4}$$

Combining this equation with the fact that $\mu_c=0$ for this case in equation (1) leads to a very simple formula for the probability of detection:

$$P_D=1-\left(1-\lambda_{th}^2\right)^{L-1} \tag{5}$$

where λ_{th} is the chosen detection threshold for declaring a change has occurred when $\hat{\mu}<\lambda_{th}$.

Using equations (15) and (4) leads to the more complicated probability of false-alarm:

---

[9] As noted in the appendix, this subsection follows [BICK15], which later was found to have unknowingly rederived a very similar methodology previously presented in the fine development in [PREIS06].

[10] In fact, as will become evident, the reason for considering the model in these three parts is to partition the problem based upon adherence to this key assumption.

$$P_{FA} = \lambda_{th}^2 \left(1-\mu_q^2\right)^L \sum_{k=0}^{L-2} \left[\left(1-\lambda_{th}^2\right)^k \, {}_2F_1\left(k+1, L, 1; \lambda_{th}^2 \mu_q^2\right) \right] \tag{6}$$

where μ_q is the population coherence of the quiescent region.

As noted in the Appendix C, there is a fairly nice recursive way to calculate equation (6). We will discuss these equations more in the section on implications.

We observe at this point that the based upon the model we have described above, the quiescent region does not change characteristics for any of the three cases described above; therefore, the probability of false-alarm for all of the resolution cases in this document will adhere to equation (6).

4.3.2 Model with change region smaller than the multilook resolution but larger than Rayleigh resolution

In this subsection, we now consider the case where the change region is a subregion within the multilook area for estimating the coherence. In other words, the change region is smaller than a multilook resolution cell, but larger than the SAR Rayleigh resolution cell size[11]. This case becomes much more complicated because we now violate the key assumption about stationarity of the coherence within our estimation window. We are mixing two different statistics within the estimation multilook resolution cell. This dictates we consider the realm of linear combinations in statistics. It is distinctly possible that an exact analytical solution to this problem does not exist; however we will use an approximation that has been developed in this field and discussed in the appendices. Limitations on the approximation will be discussed in the implications section that follows.

In this part of the CCD model we assume that the multilook resolution cell that we are using to estimate the coherence contains L SAR resolution cells of which k SAR resolution cells have the quiescent population coherence of μ_q, and $\ell = L - k$ have the change population coherence of $\mu_c = 0$. The result is that the coherence estimator for the L SAR resolution cells attempts to operate where there is a combination of the change and no-change resolution cells. We need to deal with this violation of the assumption which we made in the previous subsection.

From the discussion in Appendix A and C, we can use the multivariate Satterthwaite's approximation for the probability density function for this mixed coherence region which from the appendix permits us to use equation (3) via an approximate mixed population coherence and an approximate number of looks. The result is given by:

[11] To simplify what will become a rather complex analysis, we will make the assumption that the true change area is still some integer, ℓ, multiple of SAR resolution cells, $\ell = L - k$, where $1 \le \ell < L$.

$$p\left(\hat{\mu}\middle|(k/L)\mu_q,\nu\right)\approx 2(\nu-1)\left(1-\frac{k^2}{L^2}\mu_q^2\right)^{\nu}\hat{\mu}\left(1-\hat{\mu}^2\right)^{(\nu-2)}\,{}_2F_1\left(\nu,\nu;1;\hat{\mu}^2\frac{k^2}{L^2}\mu_q^2\right) \tag{7}$$

where the approximate change population coherence is $\mu_c \approx (k/L)\mu_q$; k, L, and μ_q are defined above and the approximate number of looks is ν is given by:

$$\nu \approx L\frac{\left[1-\left(\frac{k}{L}\right)^2\mu_q^2\right]}{\left(1-\frac{k}{L}\mu_q^2\right)\left[1+4\left(\frac{k}{L}\right)\mu_q^2\frac{\left(1-\frac{k}{L}\right)}{\left(1-\frac{k}{L}\mu_q^2\right)^2}\right]^{1/3}} \tag{8}$$

It can be observed that if $k = L$, which is the same as saying the change region equals the multilook resolution cell size, then $\nu = L$ and we end up with the same as equations as were already presented in the previous subsection, where we assumed that change region was at least as large as a multilook resolution cell size[12].

The equations in this subsection describe the probability within the multilook resolution cell that contains change. Therefore these equations are used to estimate the probability of detection which replace equation (5) above. It is also important to note that the probabilities in the quiescent (no change) regions do not change[13]. Therefore the probability of false-alarm still follows equation (6) above.

Before proceeding we wish to highlight an important point of the approximating model which is briefly discussed in Appendix A. Notice that one of the results of this choice of approximation leads to the change population coherence being a simple linear weighting of the coherences contained within the multilook resolution cell, i.e.,:

$$\mu_c \approx \left(\frac{k}{L}\right)\mu_q \tag{9}$$

This population coherence plays a major role in the change region statistics. It, along with the number of independent looks, sets the distribution within the change region. In particular, it tends to have a large influence on the mean of the coherence within the change region.

[12] Note that if $\mu_q = 0$ (which is not useful for analysis purpose) then we also end up with $\nu = L$, which is only a restatement of a known property of the central Wishart distribution (see Appendix).

[13] So important, that we will repeat and belabor this point a few times within this document.

As in the previous subsection, for the ROC curves we need the cumulative distribution. For this case, in general the ν value of is not an integer. It does not need to be an integer for the probability density function equation to be valid; however, it does need to be an integer in order to use the cumulative distribution equation above. Appendix C discusses a couple methods for handling this issue.

4.3.3 Model with change region less than Rayleigh resolution

In the case which now follows, we consider a subset (or superset, depending upon your view point) of the previous subsection, which is the case where the size of the change region is less than a radar (Rayleigh) resolution cell. We still have mixing of population coherences that occurs, but in this case we not only have mixing of two population coherences within a multilook resolution cell, as in the previous subsection, but also a mixing within a Rayleigh resolution cell. There is a distinct difference between the latter mixing and the former mixing. In the former case, the mixing occurs during, or more precisely, *because of* the coherence estimation process. The latter occurs *prior* to the coherence estimation process. The former mixing dilutes the coherence estimator, but does not affect the change population coherence within the ℓ change only resolution cells[14]. The population coherence in those cells is still zero. Conversely, when the change region is smaller than the Rayleigh resolution, the population coherence for the change region is diluted. The result is that we must repeat the analysis from the previous subsection, for $\ell = 1$ but this time $\mu_c \neq 0$.

At this point, recall that we have chosen to normalize regions to the Rayleigh resolution cell size, $\Gamma = \Gamma_c / \rho_R$. Therefore for this case we have that the size of the change region, Γ, becomes the fraction of the Rayleigh resolution cell that contains change. From the appendices, this results in an approximate change population coherence within the multilook resolution cell in this case of:

$$\mu_c = \left(1 - \frac{\Gamma}{L}\right)\mu_q \tag{10}$$

The number of looks for this case is very complicated. The method for finding the number of looks is outlined in Appendix C.

[14] This is the reason for the previous assumption of an integer value for ℓ and k .

This page left intentionally blank.

5. Adjustment to the analytical model

Key concepts in this section: We can think of the model in the previous section as a "fit" of a statistical model to certain parameters. In the multivariate case, we have several parameters from which to choose to set the fit. This section briefly discusses a more heuristic alternative choice.

In this section we very briefly discuss an alternative to the analytic model presented in the previous section (refer to Appendix B). This is a slight adjustment to the model where we use a different parameter for the "fit". We maintain the assumption of a central Wishart distribution for the mixed population coherence from the previous section. The difference is that we fit the degrees-of-freedom, also known as the effective number of looks in a different manner. We suggest that we fit the number of looks by matching the variance of simulated data to that of sample coherence that is not mixed. As in the previous case, we assume that the population coherence is the same linear weighting of the two mixed coherences.

We note that we mention this adjustment in just a few places in this document and make only limited further use of it.

This page left intentionally blank.

6. Implications from the analytical model

Key concepts in this section: The analytical model for smaller change regions presented above is an approximation, which although not perfect is reasonable. Note that it is only the probability of detection and not the probability of false-alarm that changes with resolution in this model for a fixed quiescent coherence and number of independent looks. If all other things are equal, under the assumptions of this model and other practical considerations, there is benefit for detection in estimating the coherence over the entire change region. Independently, there is benefit for reducing false-alarm by using a very large window for estimating the coherence of the quiescent (no change) region.

This section shows results of using the model and what it reveals about the CCD performance as a function of resolution for the three resolution cases of the model that were discussed in the previous section. This section also discusses the limitations of the CCD model due to approximations in the math.

In the following subsections, we now examine the effect of resolution on CCD based upon performance given by ROC curves developed from our model. We provide comparison of the model with simulation results. We start by examining the model for each of the three cases of the model. We follow this with a more general discussion of the implications of the model as a whole.

6.1 Results and implications for model with change region larger than multilook resolution

The first case we examine is the case when the change region is larger than the multilook estimation window size. As noted in the appendix, although this analysis was developed independently, it follows very closely with the previous results found in [PREI06]. The equations for the ROC curves for this case are given by equation (5) and equation (6) above. Based upon these equations, the following Figure 3 through Figure 7 show the ROC curves for different numbers of independent looks. Be sure to pay attention to the scale of the abscissa.

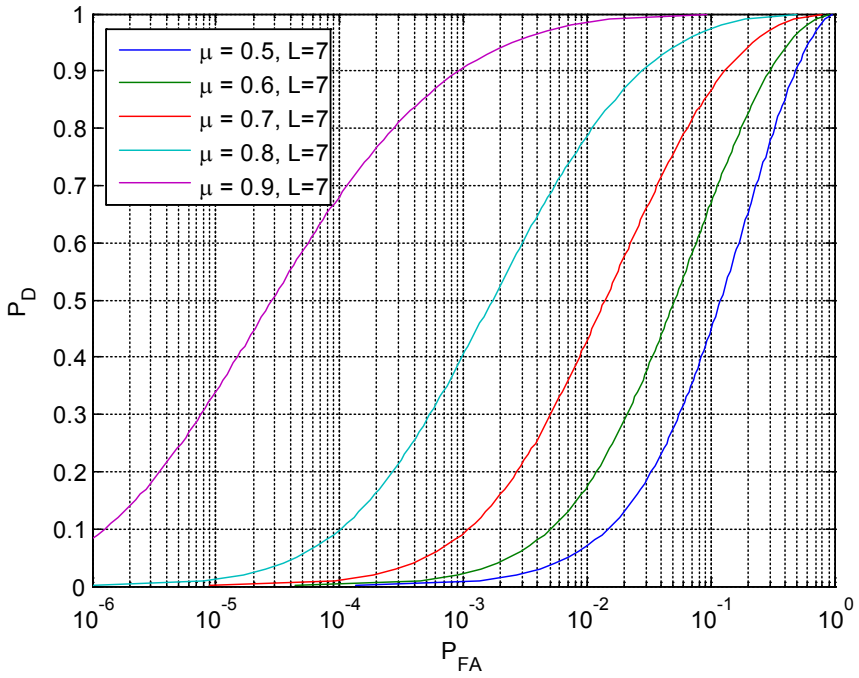

Figure 3: ROC curve for L=7 independent look for the case where the change region is larger than the multilook resolution ($\Gamma \geq L$)

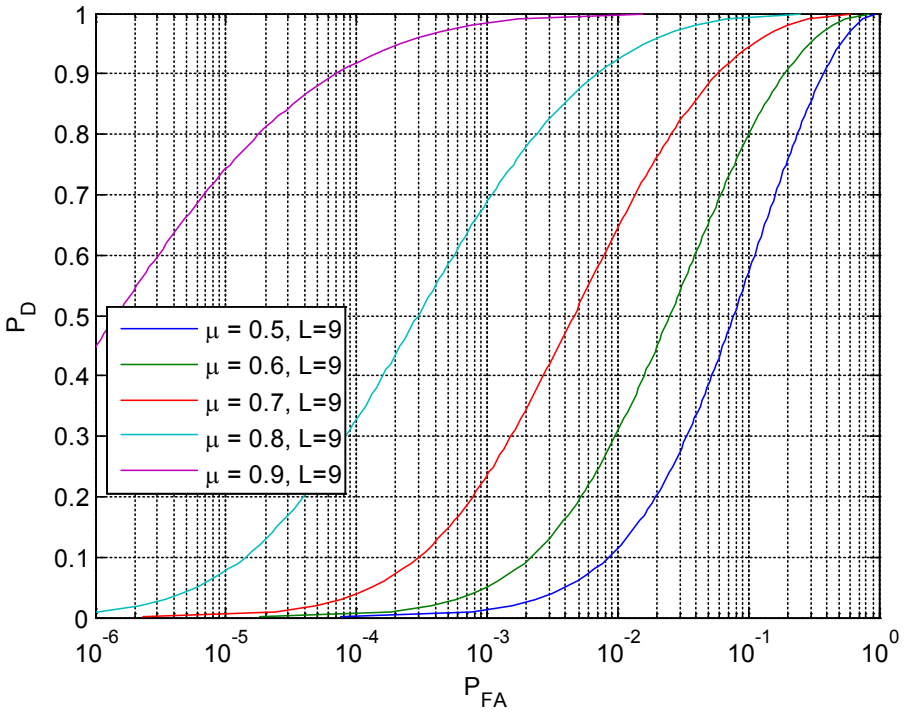

Figure 4: ROC curve for L=9 independent look for the case where the change region is larger than the multilook resolution ($\Gamma \geq L$)

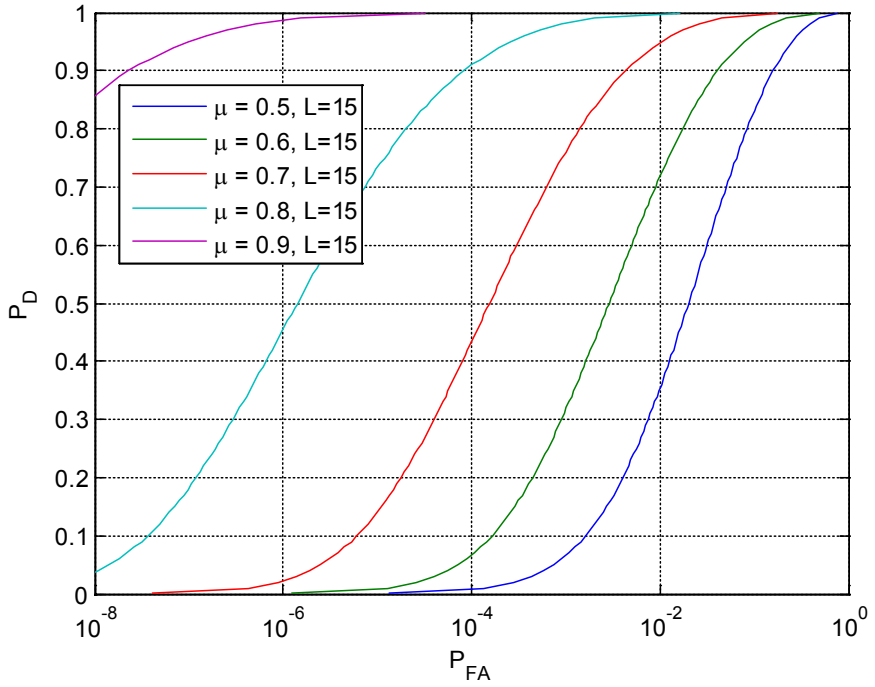

Figure 5: ROC curve for L=15 independent look for the case where the change region is larger than the multilook resolution ($\Gamma \geq L$)

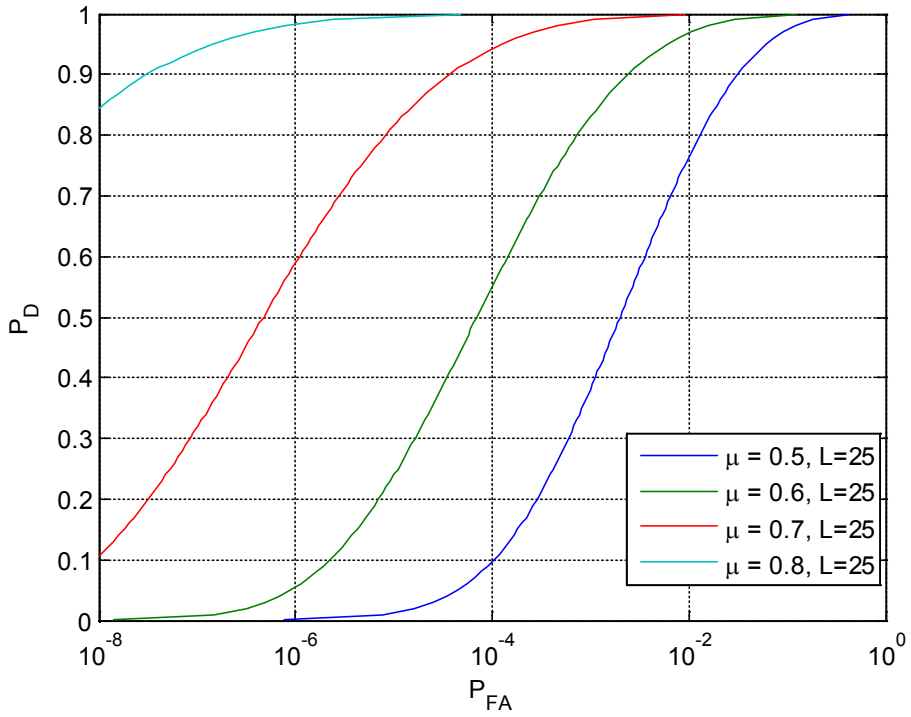

Figure 6: ROC curve for L=25 independent looks for the case where the change region is larger than the multilook resolution ($\Gamma \geq L$)

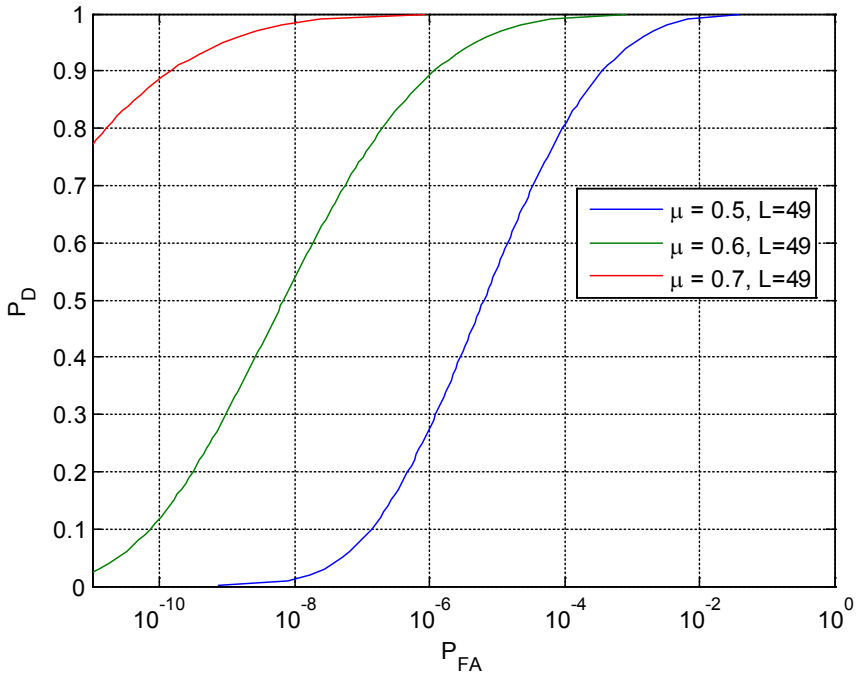

Figure 7: ROC curve for L=49 independent looks for the case where the change region is larger than the multilook resolution ($\Gamma \geq L$)

An obvious observation from the figures is that increasing the number of independent looks improves the ROC curve performance. Since we have assumed in this document that the multilook resolution cell size is $\rho_{ML} = L\rho_R$, and we have assumed for this case that the change region is at least the size of a multilook resolution cell; therefore, these imply that if we wish to improve the P_D / P_{FA} we need to either consider larger regions of change, or go to finer radar resolution. At this point we recognize that we have not presented the entire story for all of the cases; however, intuitively we expect these implications will continue to prevail.

For this case, it is very simple from equation (5) to set a specific probability of detection for a given number of independent looks by solving for the threshold as:

$$\lambda_{th} = \sqrt{1-\left(1-P_D\right)^{1/(L-1)}} \tag{11}$$

Unfortunately, in detection it is usually more important to fix the probability of false-alarm rather than the probability of detection. This leads to a common technique in detection theory called constant false-alarm rate (CFAR). In CCD, the false-alarm rate is a function of the number of independent looks, and the quiescent population coherence of the surrounding clutter, μ_q. Typically we have little control of μ_q other than taking care to keep it as high as possible [BICK14]. In standard CFAR, we adjust the threshold based upon the estimated background noise. The analog of the background noise in CCD is the quiescent coherence statistics of surrounding cells. However, in CCD, we can

control the false-alarm rate not only through the statistics of the surrounding cells but also the number of looks. Unlike in standard CFAR we will show that we can maintain the P_D if we adjust the number of looks.

Solving for this CFAR condition is complicated by the transcendental equation (6). We do this numerically in Figure 8 to show the resulting P_D given the required quiescent population coherence required to meet a constant false-alarm rate of $P_{FA} = 10^{-5}$ for 15 and 25 independent looks.

We noted above that we can also perform CFAR in this case by adjusting the number of independent looks based upon the estimate of μ surrounding the detection area[15]. In theory this should permit maintaining the P_D in the presence of CFAR. There is additional cost of loss of multilook resolution, and guard cell size, etc. An example of this is illustrated in Figure 8. We plot the number of independent looks required versus the population coherence of the clutter to maintain a fixed $P_D = 0.9$ with either a fixed $P_{FA} = 10^{-5}$ (blue line) or $P_{FA} = 10^{-6}$ (red line).

Recall that the false-alarm rate is only a function of the quiescent population coherence and the number of looks; therefore, the preceding CFAR concepts apply to all of the resolution cases. The difference will be that increasing the number of looks may push us into one of the other resolution cases which affects our consideration of the probability of detection.

6.2 Results and implications for model with change region smaller than the multilook resolution but larger than Rayleigh resolution

The implications of the previous subsection are that increasing the number of looks, L, improves probability of detection and probability of false-alarm. While it is true that increasing the number of looks reduces the false-alarm rate, it also coarsens the multilook resolution. At some point increasing the number of looks will increase the multilook resolution to the point where it becomes larger than the change region. When this occurs we violate the assumption that the change region is larger than or equal to the multilook resolution. We need to consider the second case of the model.

In this subsection, we consider the model case where the change region is smaller than the multilook resolution cell but larger than the SAR Rayleigh resolution cell size. This implies that applying the multilook window to estimate coherence in the region of change will contain both change and no-change statistics which dilutes the probability of detection. Based upon this, we will anticipate a loss of performance which we should be able to recover by finer resolution, all other things remaining equal.

[15] Adjusting the number of looks is not a new concept and has been suggested years ago for interferometric SAR applications. I have not seen it applied to CFAR detection in CCD before now. However, certainly these concepts are related.

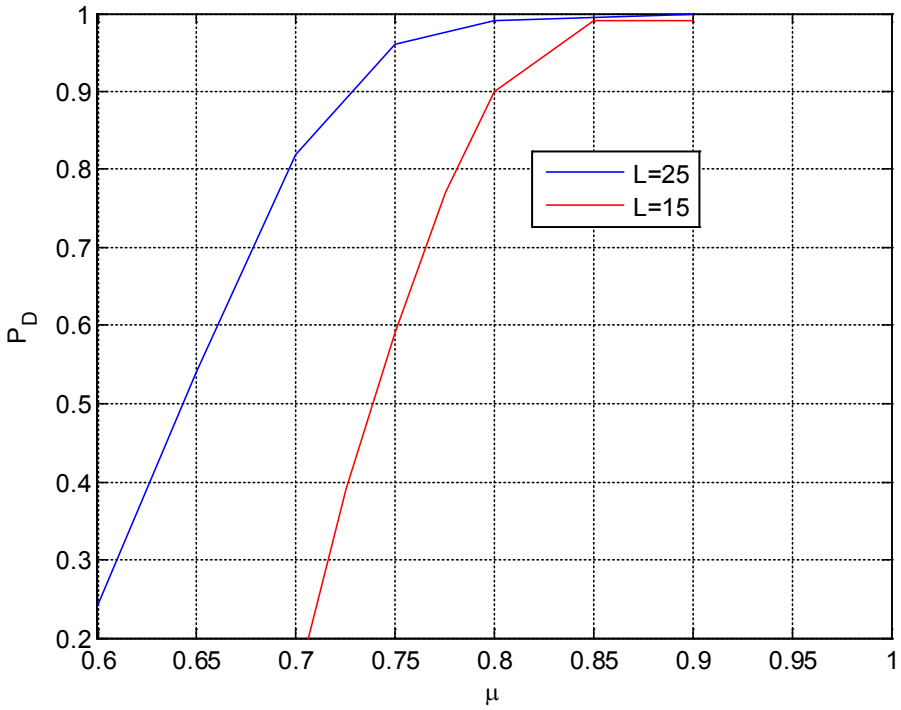

Figure 8: Probability of detection vs clutter coherence for fixed $P_{FA} = 10^{-5}$ with $L = 15$ and $L = 25$

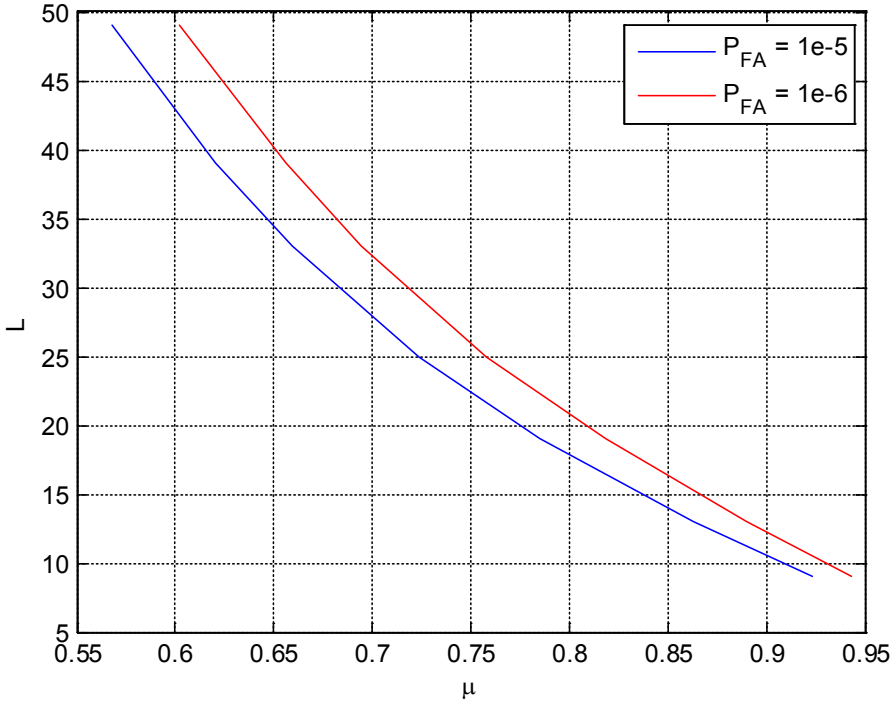

Figure 9: Number of independent looks to maintain $P_D = 0.9$ and P_{FA} versus μ_q

Before we look at the results of the model for this case, recall that our model for probability of detection is based upon an approximation to the distribution in this region that mixes samples from the change population with samples from the no change population. We wish to briefly examine how well the approximating probability describes the true probability. We do this by comparing the approximating distribution with results from simulation. We look at the distributions for varying values of ℓ from L, i.e., the fraction of the multilook resolution cell which is drawn from the change population. We also examine this approximation as a function of the quiescent population coherence.

We offer up Figure 10 as a representation of what we generally see in the approximations in the form of the cumulative distribution function. For the Satterthwaite method discussed in the subsection 4.3.2 and appendices, the approximation curve crosses the simulated curve near the mean mixed value and is symmetric about the simulated curve. The slope of the approximation is steeper than the simulated data near the mixed mean value. This leads to the approximation being slightly optimistic for higher values of the estimated coherence, and slightly pessimistic for lower values of the estimated coherence.

The matched variance method from Section 5 crosses closer at the edges of the curve, rather than the middle. The slope is flatter than the simulated data in the middle, and it tends to be more conservative.

I have noticed the general trends stated above for various simulations. It is important to note that Figure 10 does not indicate that one method or the other is always better, or that one or the other may be much different than the simulated data. Since this is the case, we will focus on the Satterthwaite's multivariate approximation and recognize for the higher values of the probability of detection it can be optimistic[16].

Recall according to equation (9) that the population coherence for the change region is a weighted function of the number of change resolution cells within a multilook resolution cell. To emphasize this, Figure 11 illustrates this for the case of $\mu_q = 0.9$ and $L = 25$ with varying values the change area, $\Gamma = \ell$ where $1 < \ell < L$. Note that the slope of this curve is proportional to the quiescent population coherence, μ_q, due to the weighting.

The result of the increase in change population coherence is that detection probability is reduced. This reduction is a function of the quiescent coherence; however, as we saw in the previous subsection, the probability of false-alarm decreases when this occurs. We will examine this relationship more in a moment.

[16] The reason for this choice might be considered somewhat arbitrary, but is used because it is based upon a known mathematical approximation and that it has a consistent mathematical formulation.

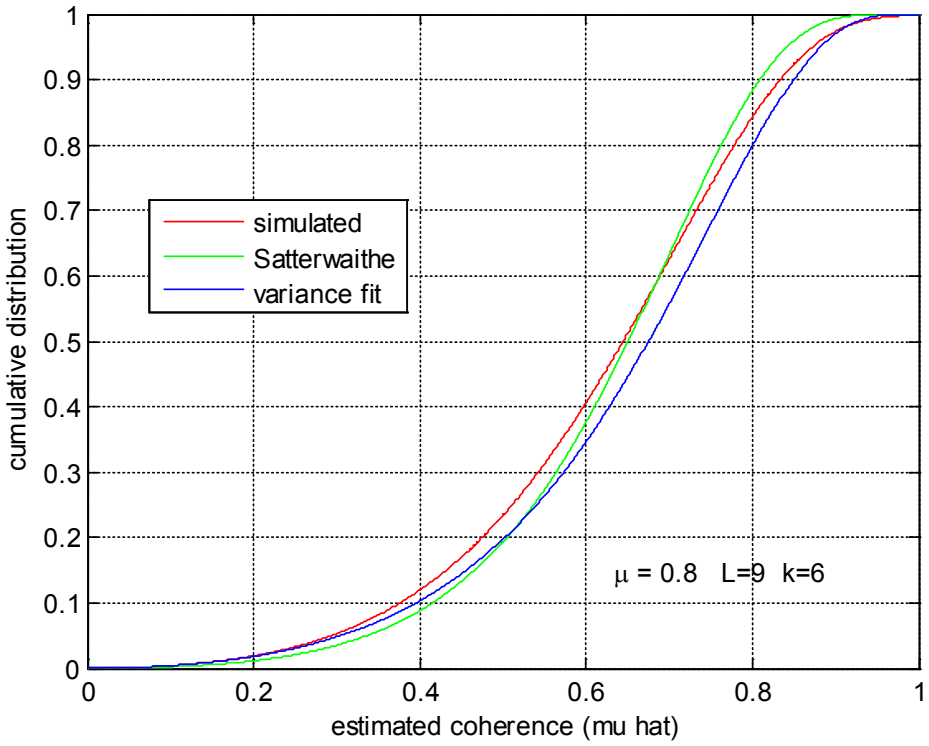

Figure 10: Cumulative distribution of $\hat{\mu}_c$ from simulation versus approximations

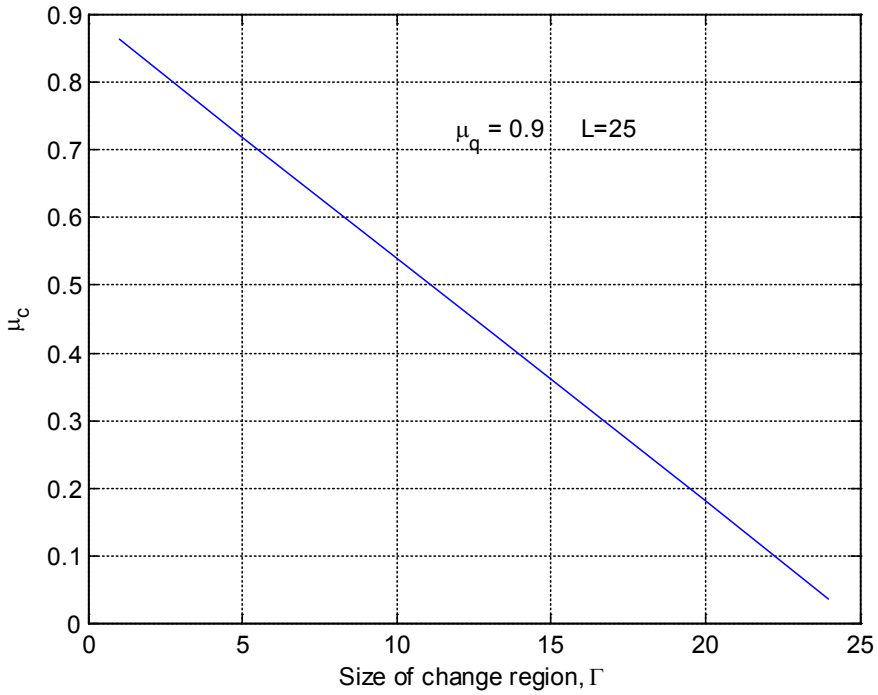

Figure 11: Plot of change population coherence versus normalized size of change region out of an $L = 25$ look multilook resolution cell

Figure 12 illustrates the effect on detection performance as the fraction of the of the radar resolution cells which contain change within a multilook resolution, ℓ/L, decreases. As ℓ/L decreases the change region within the multilook estimator becomes more diluted with surrounding quiescent coherence (radar) resolution cells. From the figure, as ℓ/L decreases, the false-alarm rate increases fairly dramatically for a given detection probability. As noted above, it is not really the false-alarm rate that has changed; rather, it is that the threshold had to be increased dramatically to maintain a given probability of detection. We also recall that for typical detection implementations we wish to maintain a constant false-alarm rate, which leads to a significant reduction in probability of detection as the change region becomes more diluted within the multilook estimation window.

We continue our investigation further by next looking at the results with a quiescent population coherence, $\mu_q = 0.7$ while maintaining the same number of looks, $L = 25$. This is depicted in Figure 13.

An interesting note is that for a given threshold and dilution, i.e., ℓ/L, the probability of detection is actually better for the $\mu_q = 0.7$ than for the $\mu_q = 0.9$. Recalling discussion from above, this is because the change population coherence is proportional to the quiescent population coherence for a given ℓ/L. The result is that the change coherence dilutes at a slower rate when mixed with a lower quiescent coherence, and vice versa, it dilutes at a faster rate when mixed with a higher quiescent coherence. The result is that probability of detection is more corrupted when then surrounding coherence is higher and the multilook resolution cell is larger than the size of the change region. However, as it was observed in the previous subsection, the probability of false-alarm increases at a faster rate when the quiescent coherence is lower. The combined result is a loss in the ROC curve performance in the lower background coherence case.

Before leaving this section, we want to compare this case with the previous case. The next few figures show the $\ell = 25$ (i.e.,the previous case where the change regions is at least as large as the multilook resolution), $\ell = 24$, $\ell = 23$ and for different population coherence values and $L = 25$. These plots use the approximation for $\ell < 25$. Even though we have shown that the approximation is slightly optimistic, from these figures the relative behavior is generally what we would intuitively expect.

We will consider more about this case in the subsection on implications.

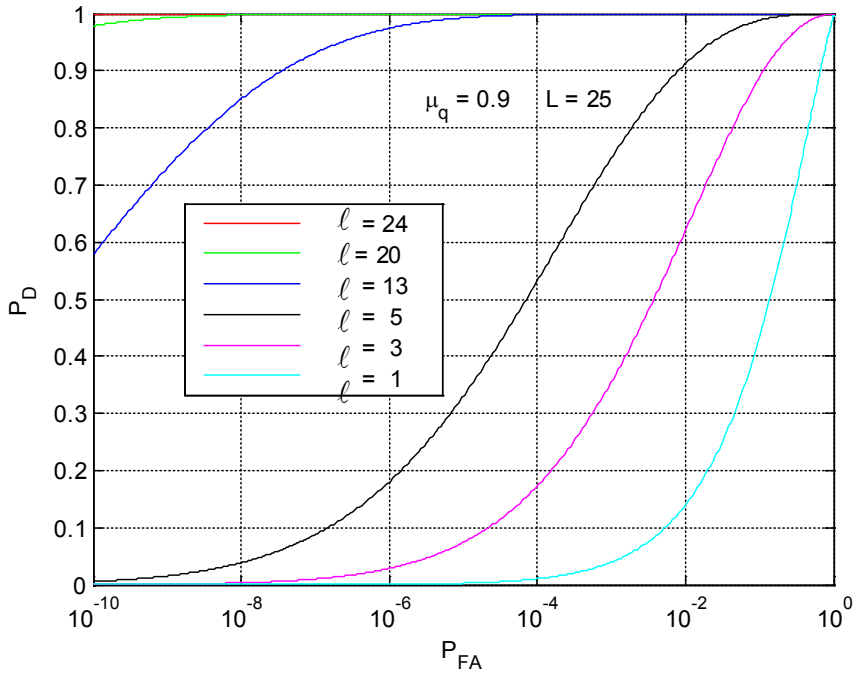

Figure 12: Plot of ROC curve for varying (normalized) size of the change for $\mu_q = 0.9$ and $L = 25$

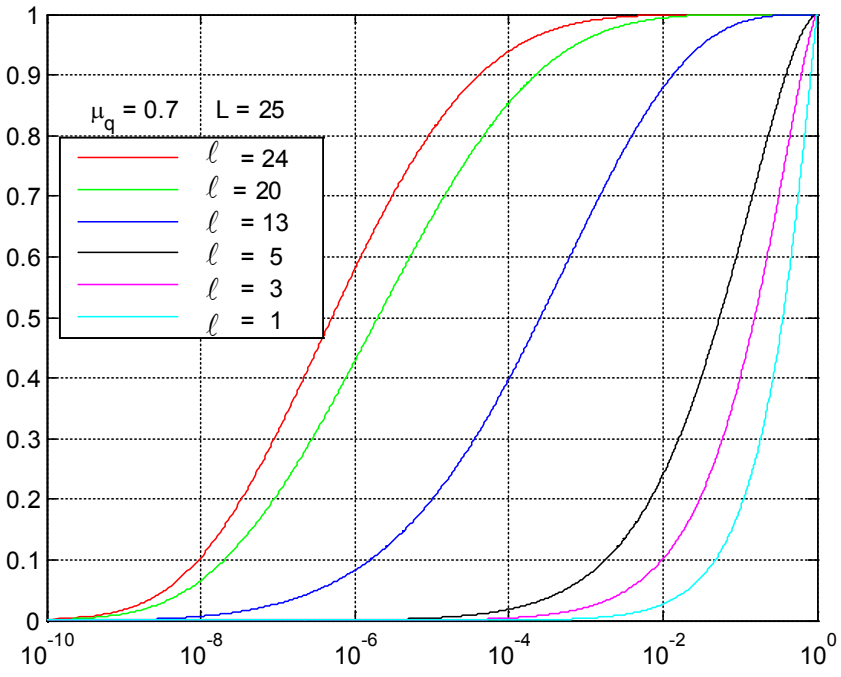

Figure 13: Plot of ROC curve for varying (normalized) size of the change for $\mu_q = 0.7$ and $L = 25$

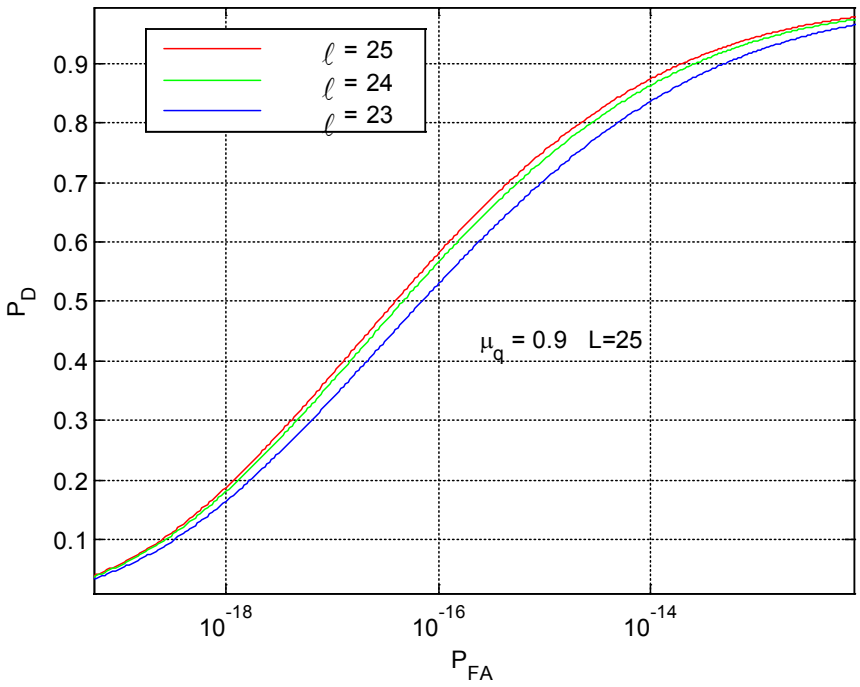

Figure 14: Plot of ROC curve for varying (normalized) size of the change crossing the three cases of the model for $\mu_q = 0.9$ and $L = 25$

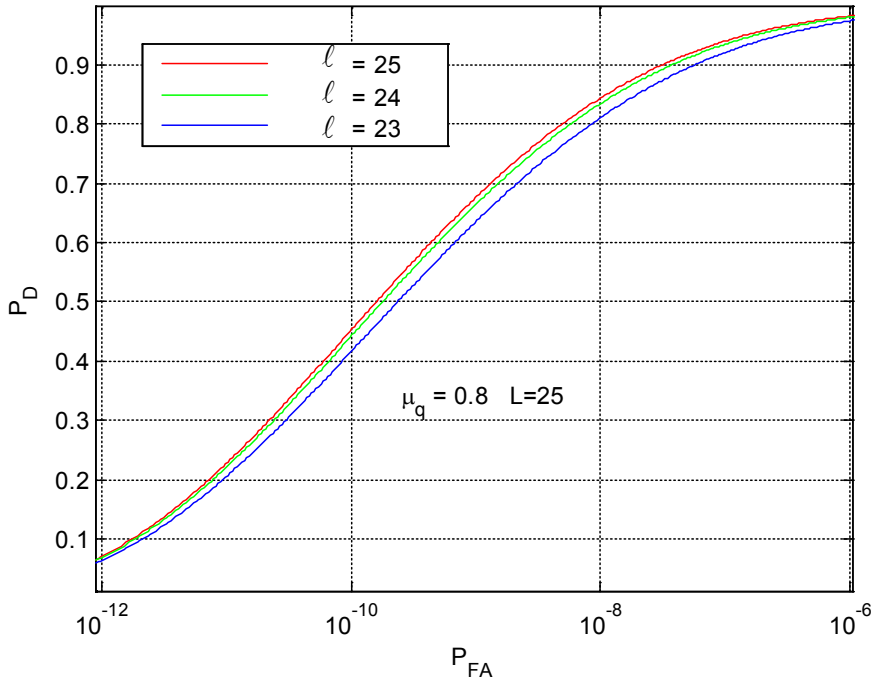

Figure 15: Plot of ROC curve for varying (normalized) size of the change crossing the three cases of the model for $\mu_q = 0.8$ and $L = 25$

6.3 Results and implications for model with change region smaller than the Rayleigh resolution

In this subsection, we consider the model case where the change region is smaller than the SAR Rayleigh resolution cell size. This leads to even further dilution of the probability of detection. Again, we anticipate loss of detection performance that can be improved with finer resolution.

We argued above that when the change region is smaller than the radar Rayleigh resolution cell size, the mixing mechanism is slightly different. The mixing within the radar resolution affects the coherence *prior* to the coherence estimation. This changes the statistics. To illustrate this further, we consider the following. Assume that some fraction of the radar resolution cell, $\Gamma < 1$, contains changes between two images. Assume that the quiescent coherence is μ_q. Then given the *key assumption* that *each* radar resolution cell within the multilook estimation cell has this same fraction of change, the probability density function is given without approximation by equation (3) with population coherence, $(1-\Gamma)\mu_q$, and L looks. Although we will not show it here for some semblance of brevity, simulation bears this out.

The approximation from the previous subsection still comes into play due to the fact that we will assume that *only one* radar resolution cell within the multilook resolution cell contains change. Therefore, Satterthwaite's approximation is used again with the weighted population coherence of the change within the multilook resolution cell is that given previously in equation (10).

As in the previous subsection, we start by looking at the effects of the approximations made in deriving the probability distribution in this "mixed" region. Figure 16 shows the approximation versus simulation for the case where the change region only covers half of a radar Rayleigh resolution cell. The results are shown for $\mu_q = 0.9$ and $\mu_q = 0.7$. Again this figure shows that the Satterthwaite's approximation is slightly optimistic but reasonable in this case.

The following figures compare the results of $\Gamma = 1$ (or $\ell = 1$ which is when the change size is one radar resolution cell) versus $\Gamma = 0.5$ (which is change size of one half of a radar resolution cell). As in the previous subsection, these plots use the model. Again, these plots follow our intuition as far as the relative behavior of the two different cases.

We want to defer the rest of the analysis of the model for this case to the next section where we will evaluate this case against the other cases.

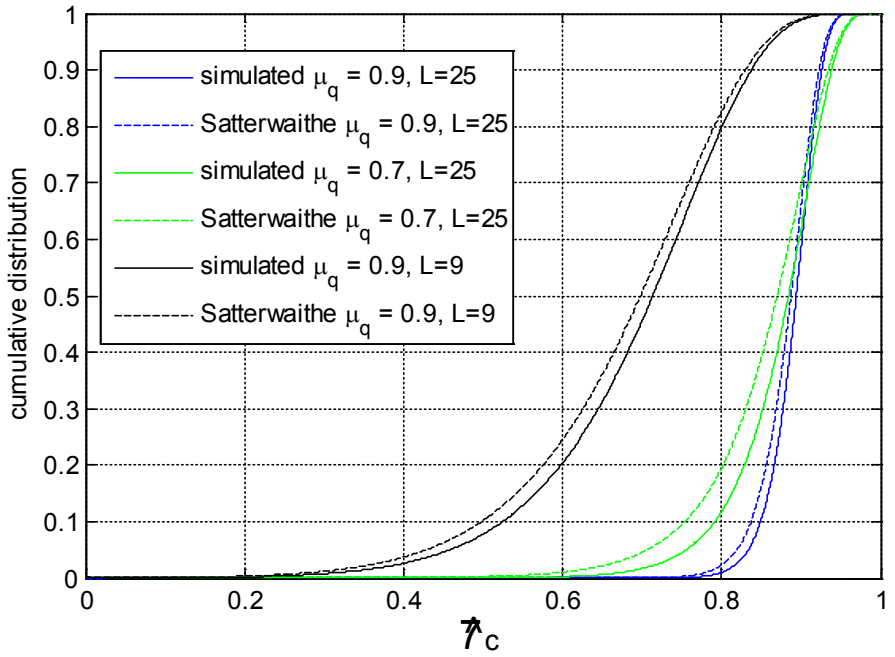

Figure 16: Cumulative distribution of $\hat{\mu}_c$ from simulation versus approximation for $\Gamma = 0.5$ and varying μ_q

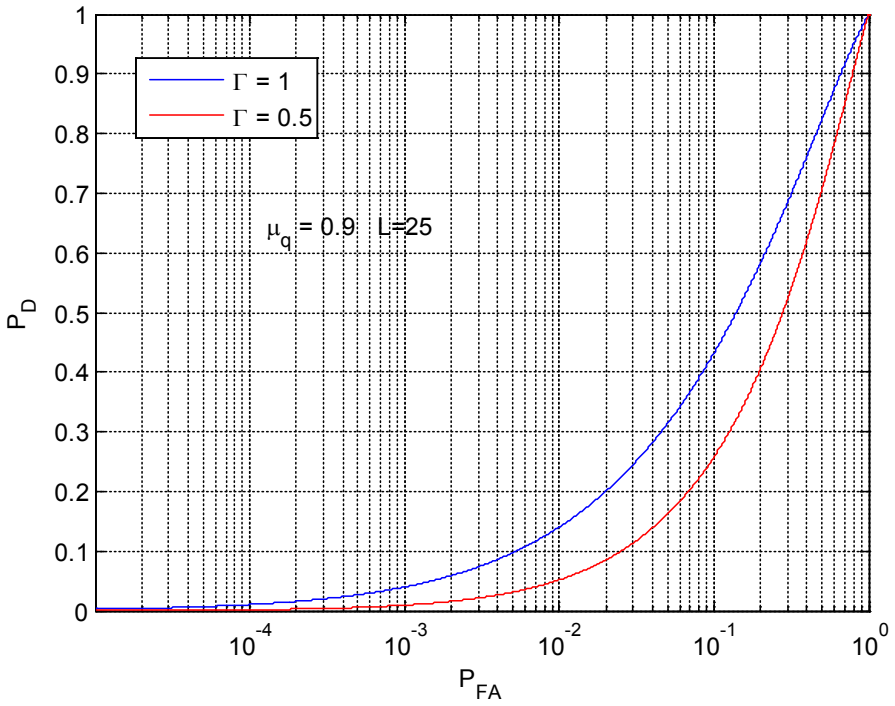

Figure 17: Plot of ROC curve for $\Gamma = 1$ (i.e., $\ell = 1$ or change size is one radar resolution cell) and $\Gamma = 0.5$ (i.e., change size is one half of a radar resolution cell) model for $\mu_q = 0.9$ and $L = 25$

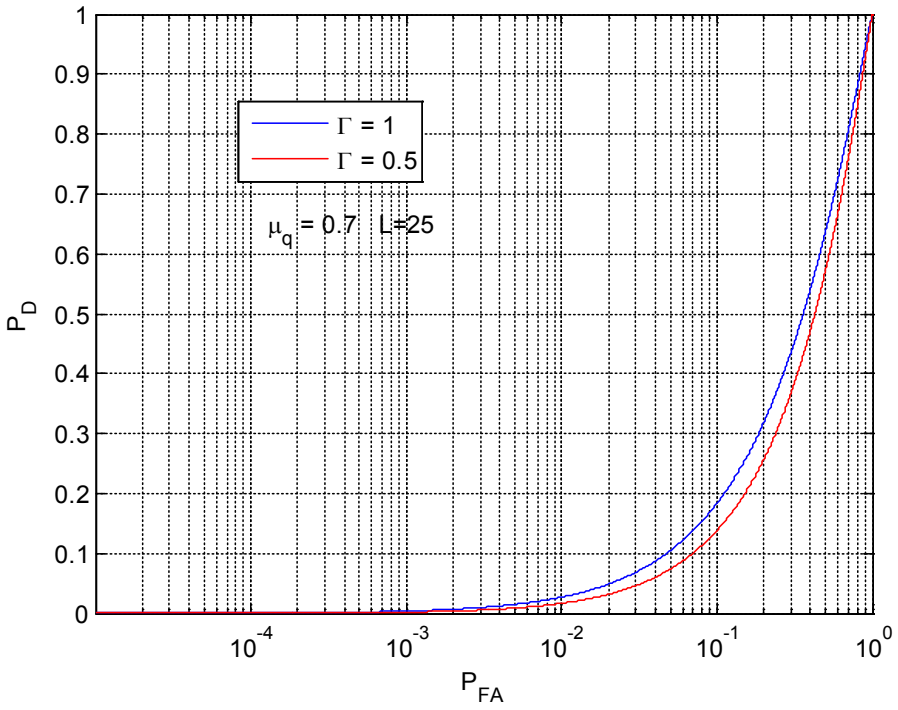

Figure 18: Plot of ROC curve for $\Gamma = 1$ (i.e., $\ell = 1$ or change size is one radar resolution cell) and $\Gamma = 0.5$ (i.e., change size is one half of a radar resolution cell) model for $\mu_q = 0.7$ and $L = 25$

6.4 General implications

In this subsection we consider the model as a whole. With apologies for repetitiveness, it is still important to remember that the probability of false-alarm does not change for the different cases. It is only the probability of detection that changes.

From the previous discussion, it is obvious that detection performance is affected by increasing the number of looks. Increasing the number of looks in the quiescent region reduces the probability of false-alarm. Increasing the number of looks in the change region increases the probability of detection *if* increasing the multilook resolution *only* includes resolution cells that contain change. Eventually increasing the number of looks causes the multilook resolution cell to exceed the size of the change region. To counter this, improving the radar resolution to finer resolution can keep this from happening. Therefore, improving resolution in this case can improve change detection. This was illustrated in Figure 9.

Next we want to look at the effect of a fixed change size and how changing the number of looks influences the performance. To examine this further we will look at how the ROC curves behave as a function of the change region size (normalized to radar resolution), multilook resolution size (also normalized by the radar resolution) and no-change region

population coherences. We present an extended sequence of figures where each figure represents a specific no-change population coherence, μ_q, and a specific (normalized) size of the change region, $\Gamma = \ell$ in this case, for varying multilook resolution cell sizes, L. In general the results are complicated, which is another way of saying that they are interesting and revealing.

We now consider a modest number of results from applying the model. Figure 19 shows the case for $\Gamma = 1$ and $\mu_q = 0.9$. Figure 20 shows the case for $\Gamma = 1$ and $\mu_q = 0.8$. Figure 21 shows the case for $\Gamma = 1$ and $\mu_q = 0.7$. $\mu_q = 0.8$. Figure 22 shows the case for $\Gamma = 1$ and $\mu_q = 0.6$. Figure 23 shows the case for $\Gamma = 1$ and $\mu_q = 0.9$. Figure 24 shows the case for $\Gamma = 1$ and $\mu_q = 0.8$. Figure 25 shows the case for $\Gamma = 1$ and $\mu_q = 0.7$. $\mu_q = 0.8$. Figure 26 shows the case for $\Gamma = 1$ and $\mu_q = 0.6$. Figure 27 shows the case for $\Gamma = 5$ and $\mu_q = 0.9$. Figure 28 hows the case for $\Gamma = 5$ and $\mu_q = 0.8$. Figure 29 shows the case for $\Gamma = 5$ and $\mu_q = 0.7$. Figure 30 shows the case for $\Gamma = 5$ and $\mu_q = 0.6$. Figure 31 shows the case for $\Gamma = 9$ and $\mu_q = 0.9$. Figure 32 shows the case for $\Gamma = 9$ and $\mu_q = 0.8$. Figure 33 shows the case for $\Gamma = 9$ and $\mu_q = 0.7$. Figure 34 shows the case for $\Gamma = 9$ and $\mu_q = 0.6$. Figure 35 shows the case for $\Gamma = 16$ and $\mu_q = 0.9$. Figure 36 shows the case for $\Gamma = 16$ and $\mu_q = 0.8$. Figure 37 shows the case for $\Gamma = 16$ and $\mu_q = 0.7$. Figure 38 shows the case for $\Gamma = 16$ and $\mu_q = 0.6$. Figure 39 shows the case for $\Gamma = 25$ and $\mu_q = 0.9$. Figure 40 shows the case for $\Gamma = 25$ and $\mu_q = 0.8$. Figure 41 shows the case for $\Gamma = 25$ and $\mu_q = 0.7$. Figure 42 shows the case for $\Gamma = 25$ and $\mu_q = 0.6$. In all of these figures, be sure to note the scale of the axes in order to understand the relative behaviors.

We point out some general observations from plots using the model. First, there is obvious loss of performance as the quiescent population coherence goes down. Second, there is an obvious improvement in the performance as the change region gets larger. Since the key parameter is the size of the change region *relative to* the radar resolution, this in turn means that if all other considerations are equal, finer resolution increases Γ and therefore improves CCD performance. Third, the optimum number of looks changes depends upon the size of the change regions, Γ. As a rough rule-of-thumb, it appears that the optimum number of looks is around 1.5 to 2 times the change region size[17].

A few more nuanced observations are discussed. The ROC curve performance is not as strong of a function of number of looks when the quiescent population coherence is reduced. Also, the ROC curve is steeper as the change region size approaches the multilook resolution cell size, i.e., as $\Gamma/L \to 1$.

[17] It appears that a minimum of $L = 4$ is needed to keep the false-alarm rate low.

We briefly return to the rule-of-thumb, which is just a rough rule-of-thumb. At first blush, it is a little surprising that this indicates that a small amount of mixing of change with the no change is reasonable. What is happening is that for the case where the multilook resolution cell size is close to the change region size, increasing the number of looks improves the false-alarm rate faster than it reduces the probability of detection. This does make sense from the perspective that for the change region the coherence is low, which leads to higher bias and variance in the estimator for this region. Therefore a small increase in the population coherence when it is near zero coherence does not create a large change in the probability density function.

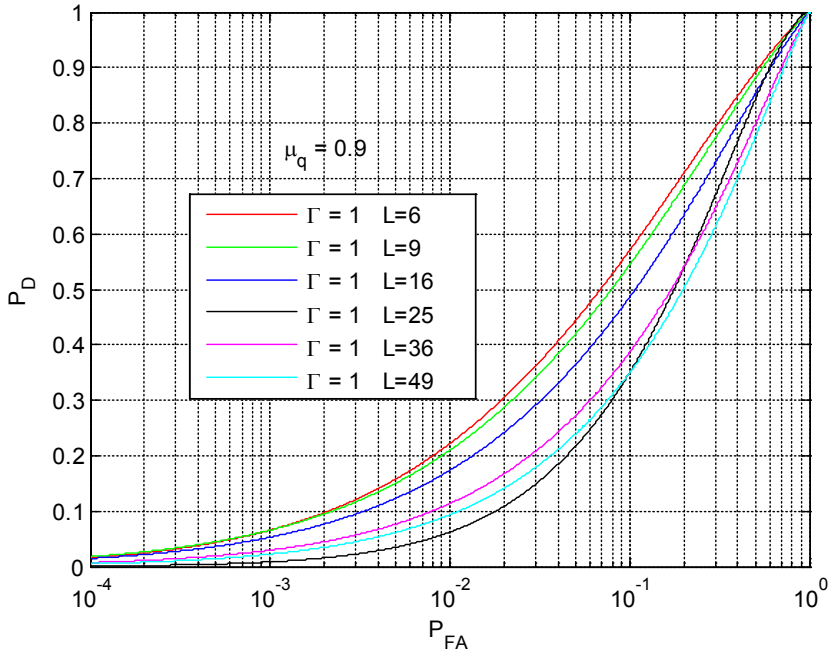

Figure 19: Plot of ROC curve for $\Gamma = 1$ (i.e., $\ell = 1$) for $\mu_q = 0.9$ and varying number of looks, $L = \{6, 9, 16, 25, 36, 49\}$

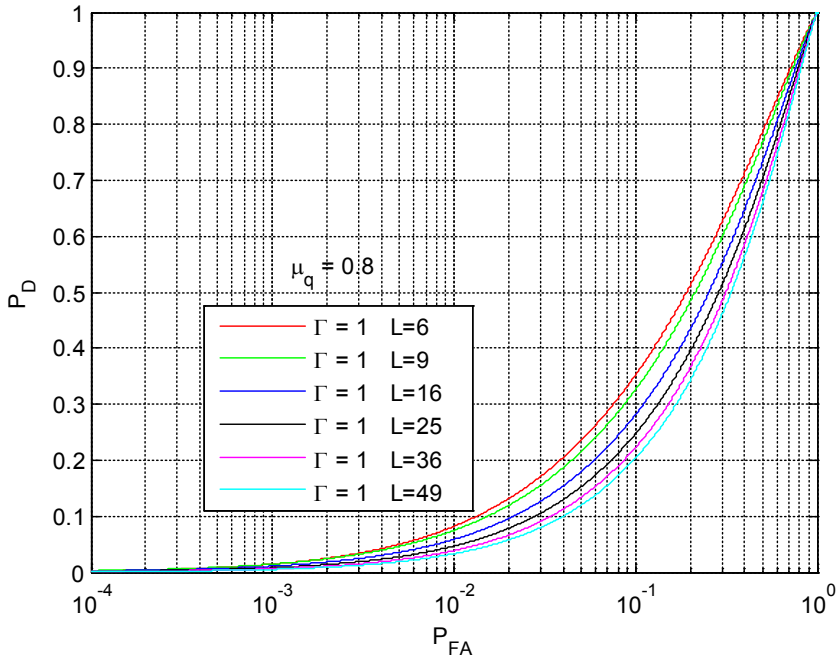

Figure 20: Plot of ROC curve for $\Gamma = 1$ (i.e., $\ell = 1$) for $\mu_q = 0.8$ and varying number of looks, $L = \{6, 9, 16, 25, 36, 49\}$

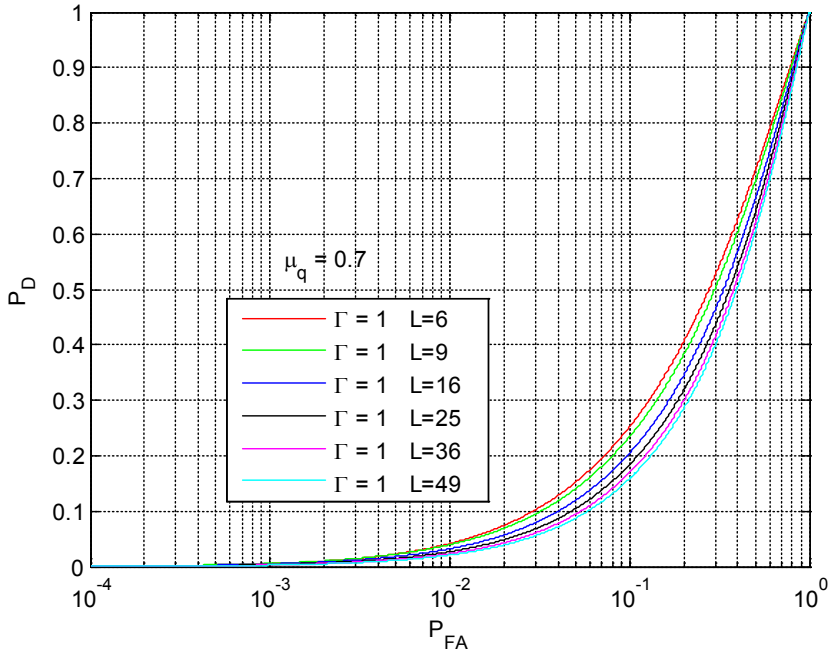

Figure 21: Plot of ROC curve for $\Gamma = 1$ (i.e., $\ell = 1$) for $\mu_q = 0.7$ and varying number of looks, $L = \{6, 9, 16, 25, 36, 49\}$

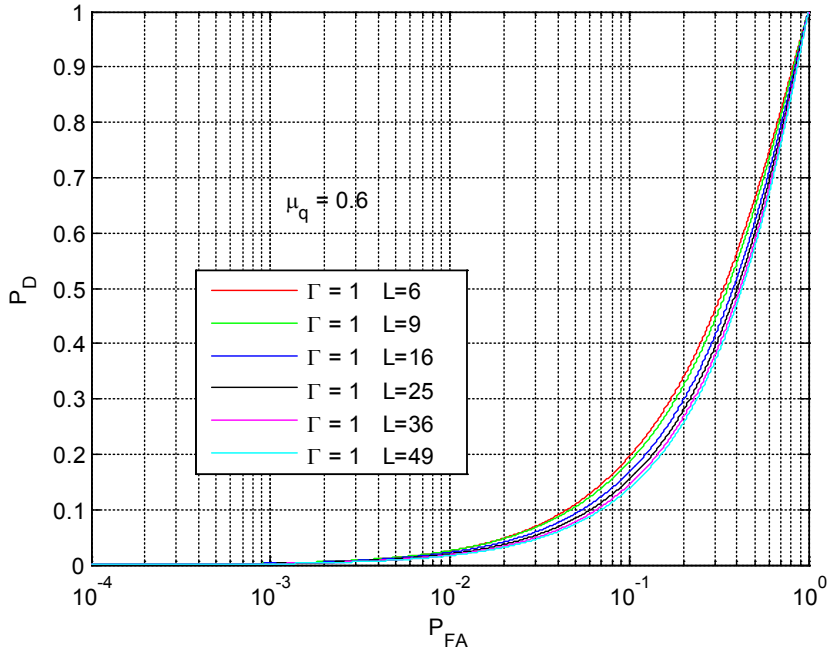

Figure 22: Plot of ROC curve for $\Gamma = 1$ (i.e., $\ell = 1$) for $\mu_q = 0.6$ and varying number of looks, $L = \{6, 9, 16, 25, 36, 49\}$

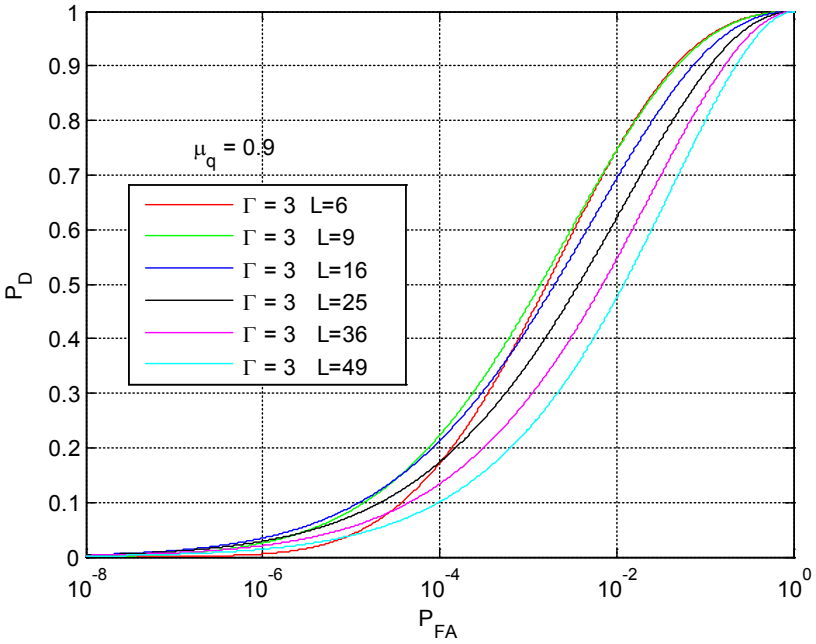

Figure 23: Plot of ROC curve for $\Gamma = 3$ (i.e., $\ell = 3$) for $\mu_q = 0.9$ and varying number of looks, $L = \{6, 9, 16, 25, 36, 49\}$

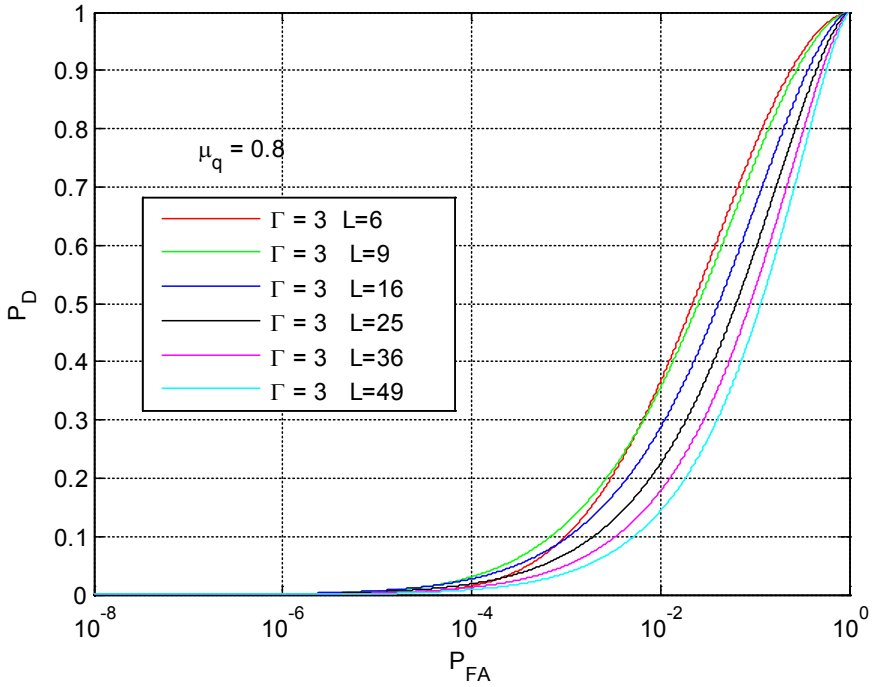

Figure 24: Plot of ROC curve for $\Gamma = 3$ (i.e., $\ell = 3$) for $\mu_q = 0.8$ and varying number of looks, $L = \{6, 9, 16, 25, 36, 49\}$

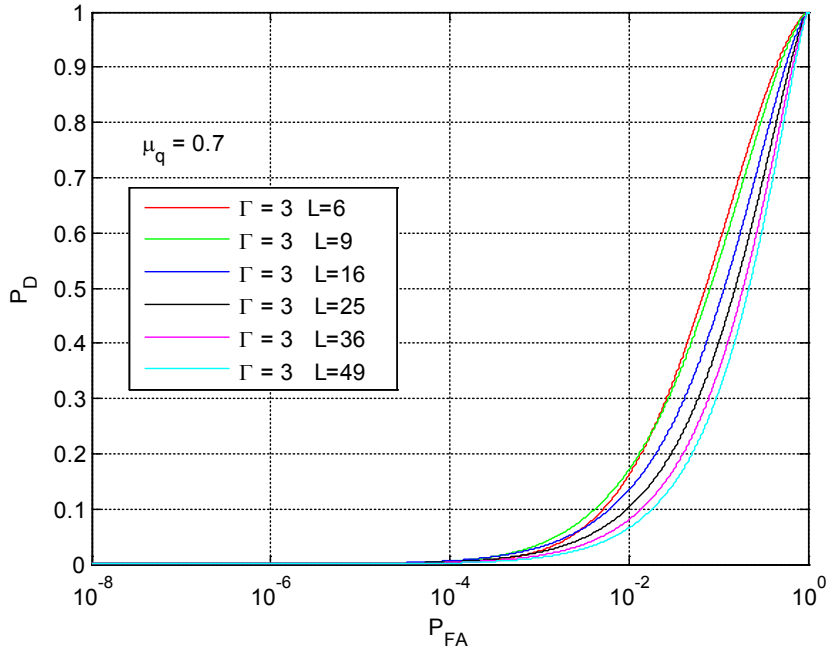

Figure 25: Plot of ROC curve for $\Gamma = 3$ (i.e., $\ell = 3$) for $\mu_q = 0.7$ and varying number of looks, $L = \{6, 9, 16, 25, 36, 49\}$

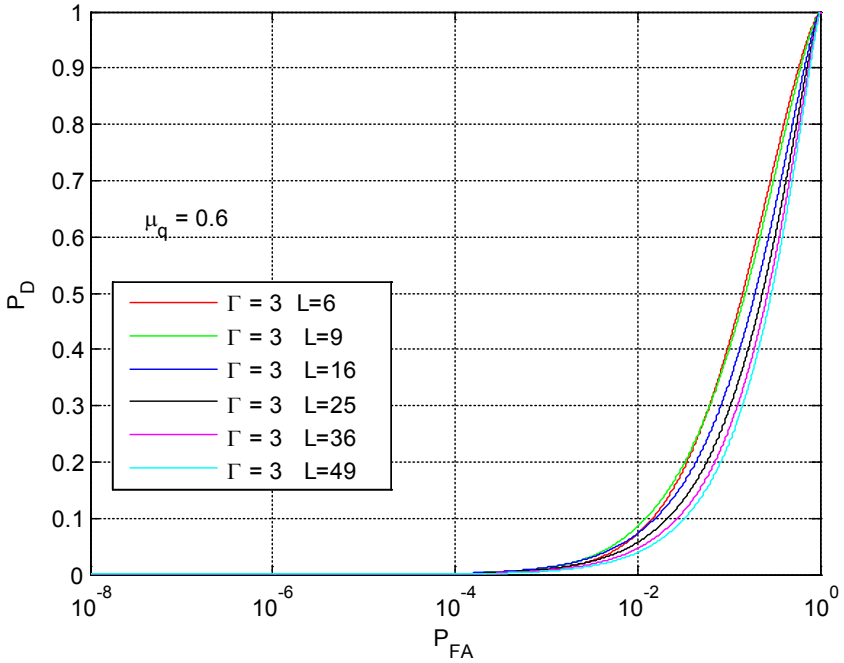

Figure 26: Plot of ROC curve for $\Gamma = 3$ (i.e., $\ell = 3$) for $\mu_q = 0.6$ and varying number of looks, $L = \{6, 9, 16, 25, 36, 49\}$

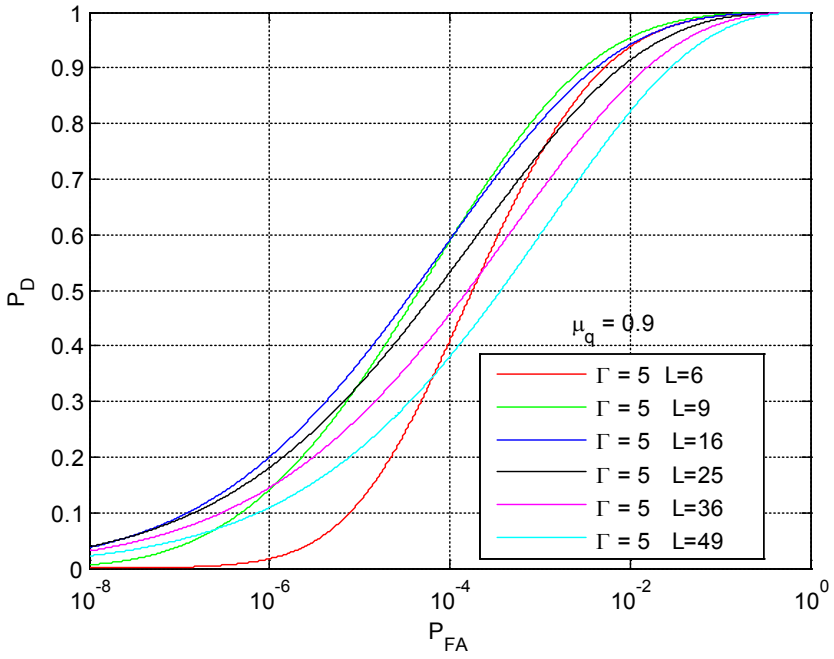

Figure 27: Plot of ROC curve for $\Gamma = 5$ (i.e., $\ell = 5$) for $\mu_q = 0.9$ and varying number of looks, $L = \{6, 9, 16, 25, 36, 49\}$

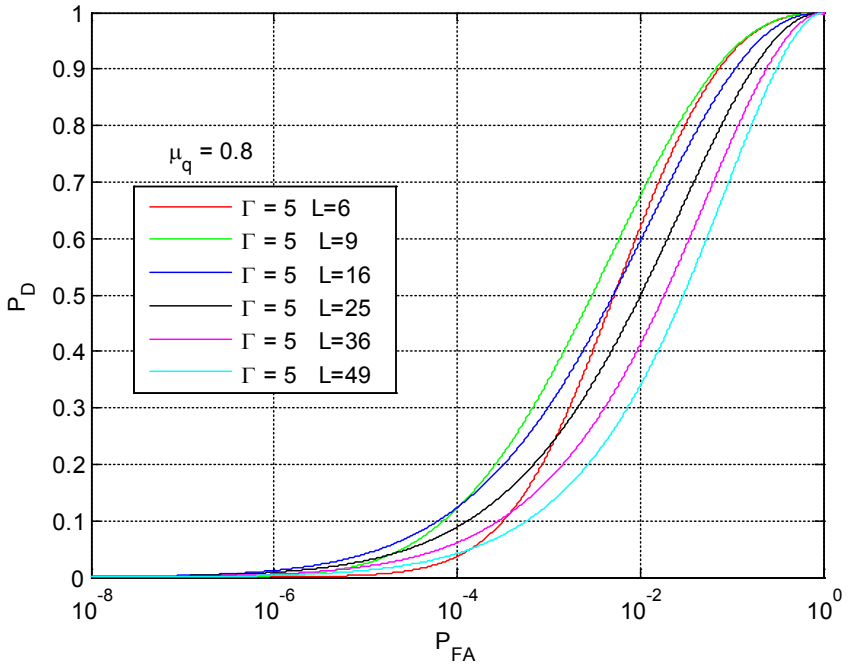

Figure 28: Plot of ROC curve for $\Gamma = 5$ (i.e., $\ell = 5$) for $\mu_q = 0.8$ and varying number of looks, $L = \{6, 9, 16, 25, 36, 49\}$

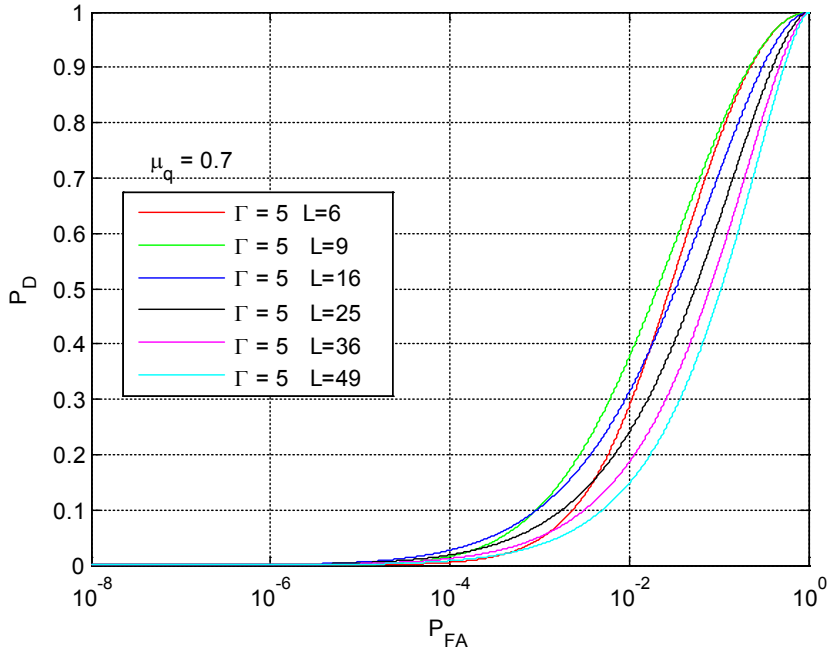

Figure 29: Plot of ROC curve for $\Gamma = 5$ (i.e., $\ell = 5$) for $\mu_q = 0.7$ and varying number of looks, $L = \{6, 9, 16, 25, 36, 49\}$

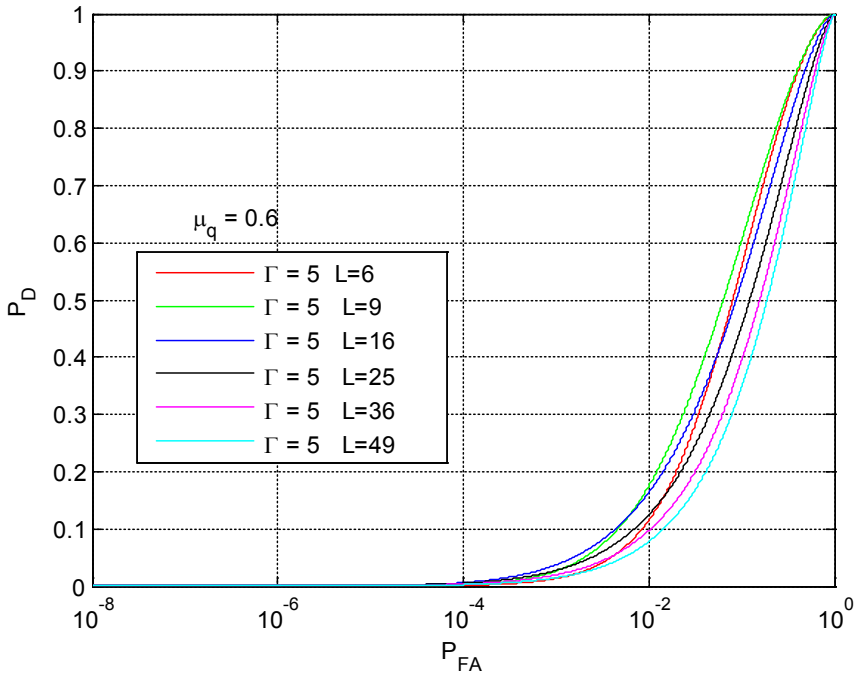

Figure 30: Plot of ROC curve for $\Gamma = 5$ (i.e., $\ell = 5$) for $\mu_q = 0.6$ and varying number of looks, $L = \{6, 9, 16, 25, 36, 49\}$

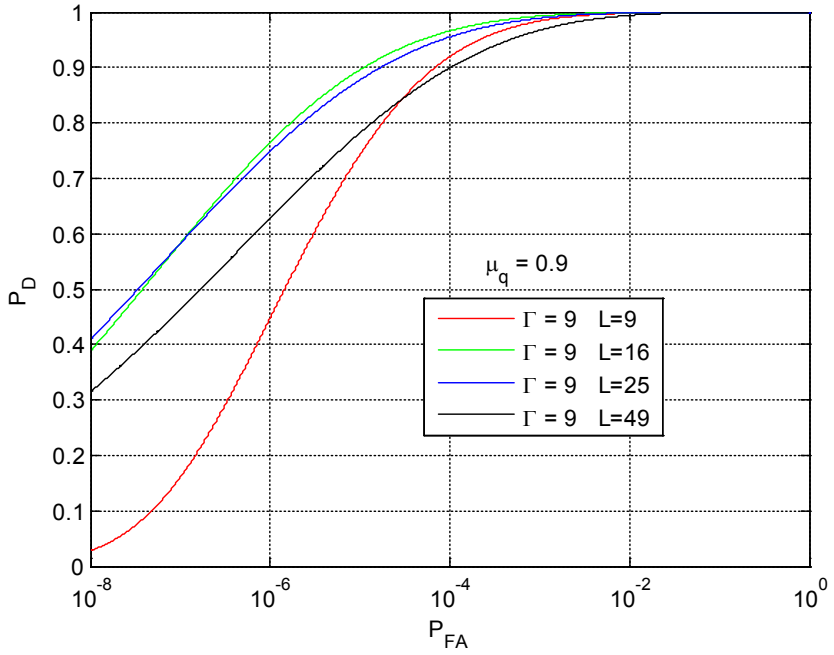

Figure 31: Plot of ROC curve for $\Gamma = 9$ (i.e., $\ell = 9$) for $\mu_q = 0.9$ and varying number of looks, $L = \{9,16,25,49\}$

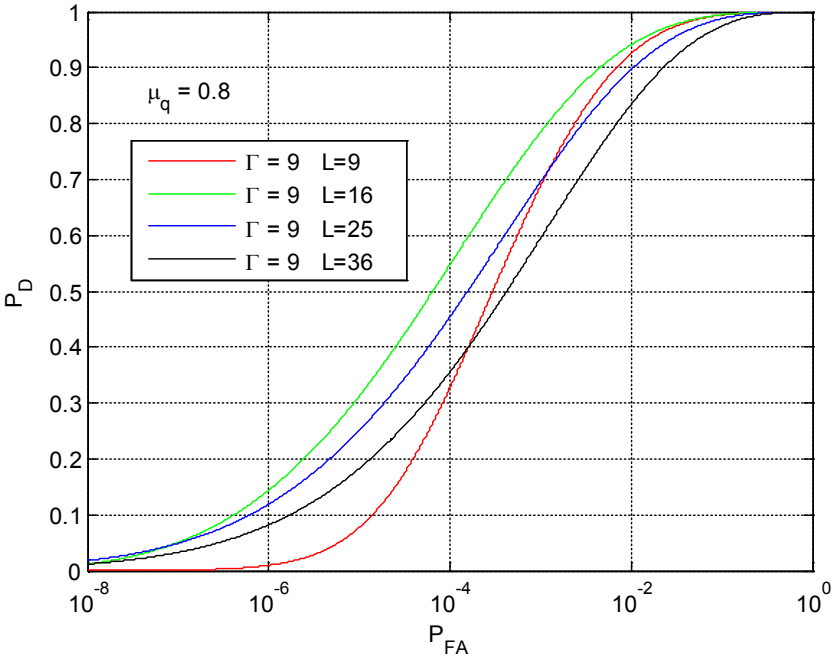

Figure 32: Plot of ROC curve for $\Gamma = 9$ (i.e., $\ell = 9$) for $\mu_q = 0.8$ and varying number of looks, $L = \{9,16,25,49\}$

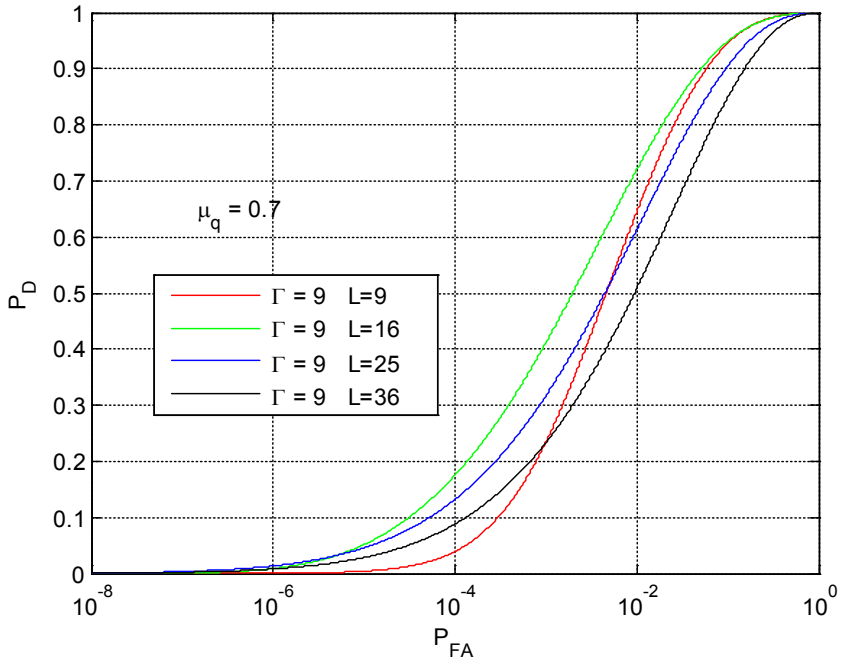

Figure 33: Plot of ROC curve for $\Gamma = 9$ (i.e., $\ell = 9$) for $\mu_q = 0.7$ and varying number of looks, $L = \{9, 16, 25, 49\}$

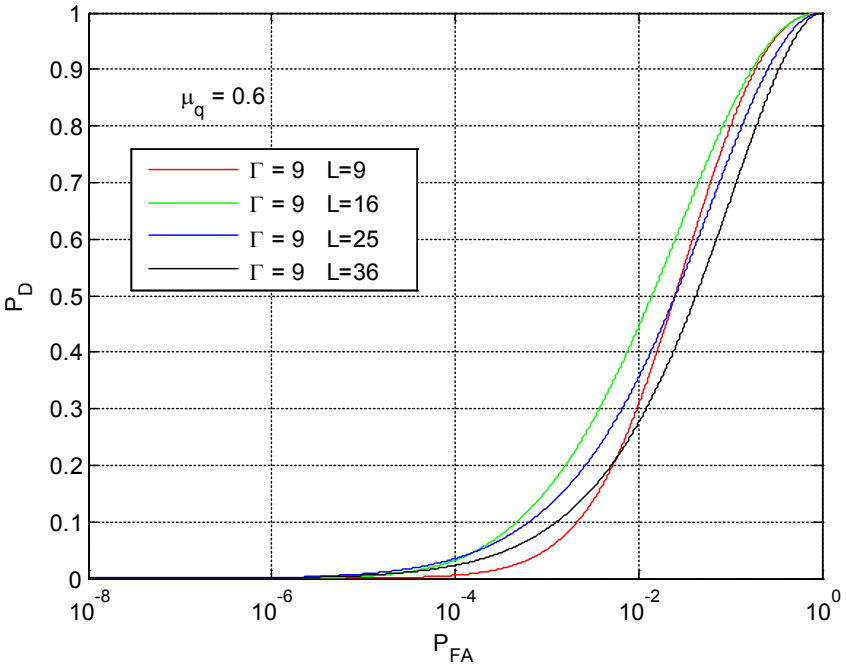

Figure 34: Plot of ROC curve for $\Gamma = 9$ (i.e., $\ell = 9$) for $\mu_q = 0.6$ and varying number of looks, $L = \{9, 16, 25, 49\}$

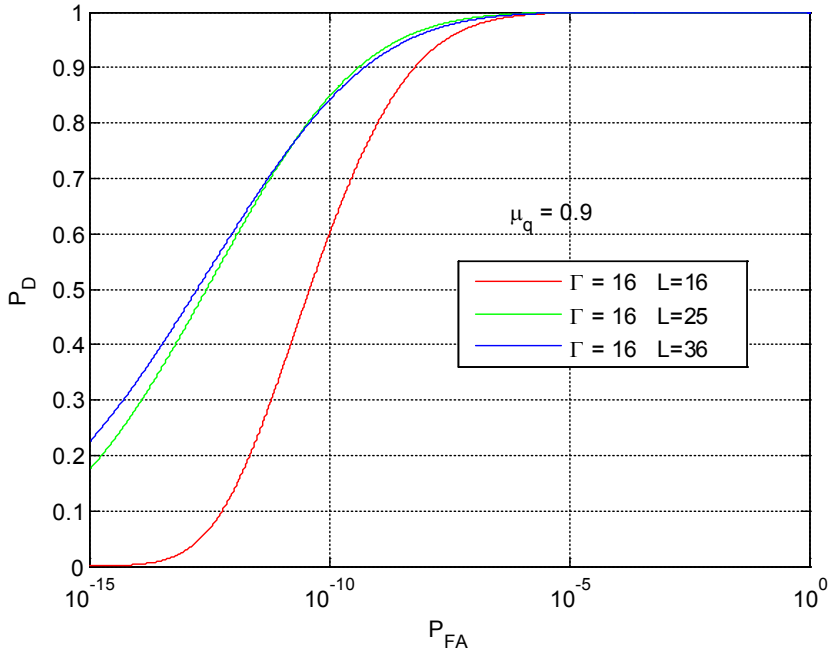

Γ=16

Figure 35: Plot of ROC curve for $\Gamma = 16$ (i.e., $\ell = 16$) for $\mu_q = 0.9$ and varying number of looks, $L = \{16, 25, 49\}$

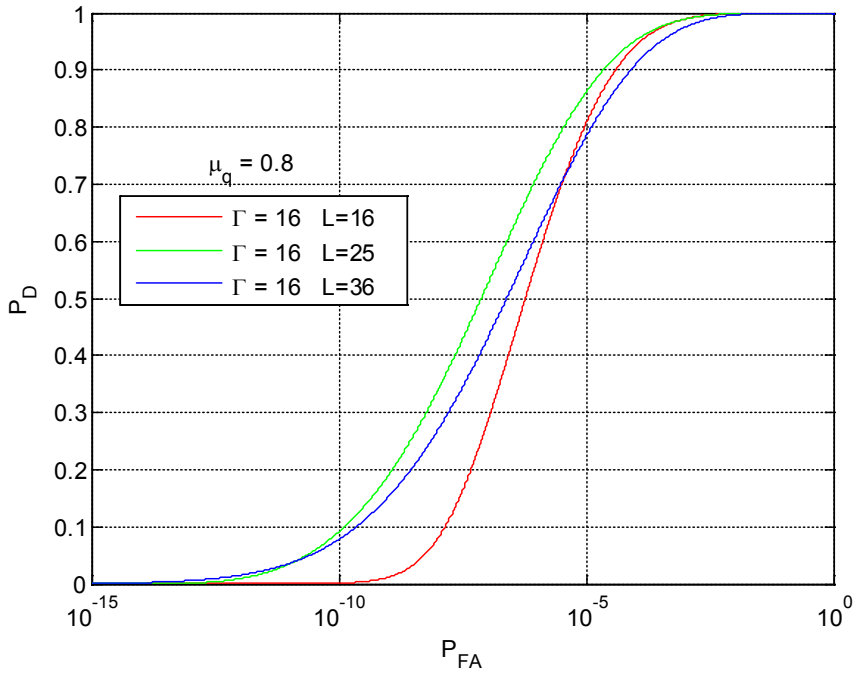

Figure 36: Plot of ROC curve for $\Gamma = 16$ (i.e., $\ell = 16$) for $\mu_q = 0.8$ and varying number of looks, $L = \{16, 25, 49\}$

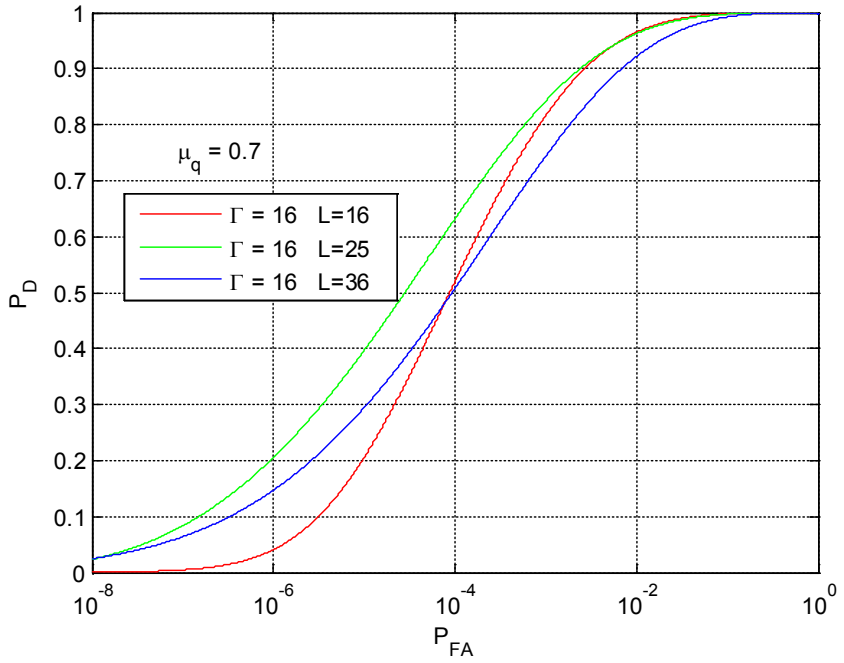

Figure 37: Plot of ROC curve for $\Gamma = 16$ (i.e., $\ell = 16$) for $\mu_q = 0.7$ and varying number of looks, $L = \{16, 25, 49\}$

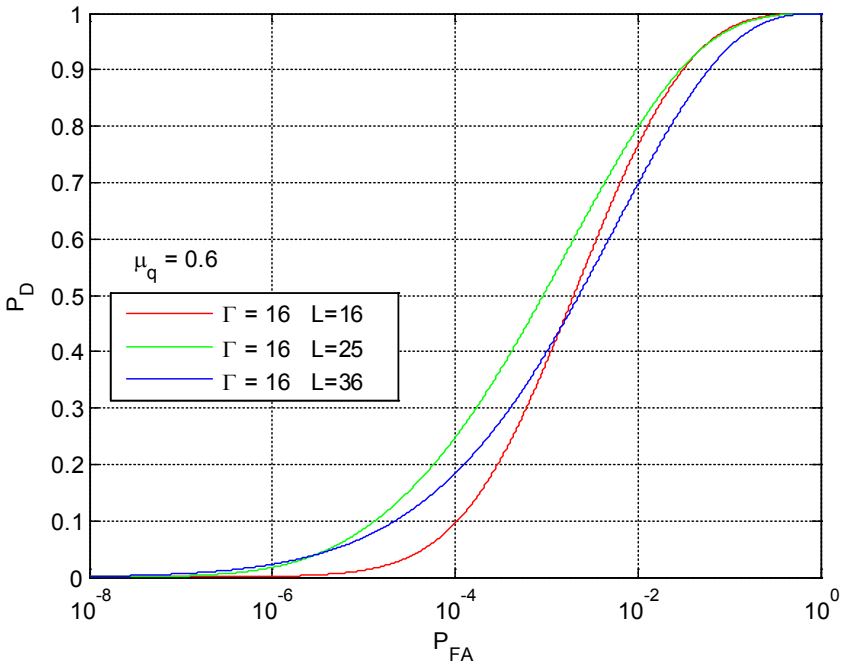

Figure 38: Plot of ROC curve for $\Gamma = 16$ (i.e., $\ell = 16$) for $\mu_q = 0.6$ and varying number of looks, $L = \{16, 25, 49\}$

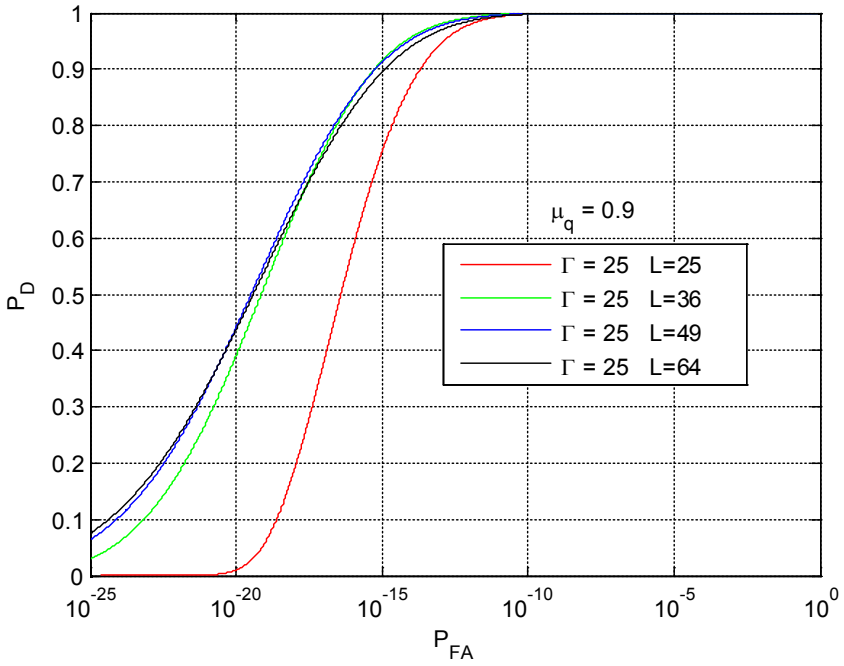

Figure 39: Plot of ROC curve for $\Gamma = 25$ (i.e., $\ell = 25$) for $\mu_q = 0.9$ and varying number of looks, $L = \{25, 36, 49, 64\}$

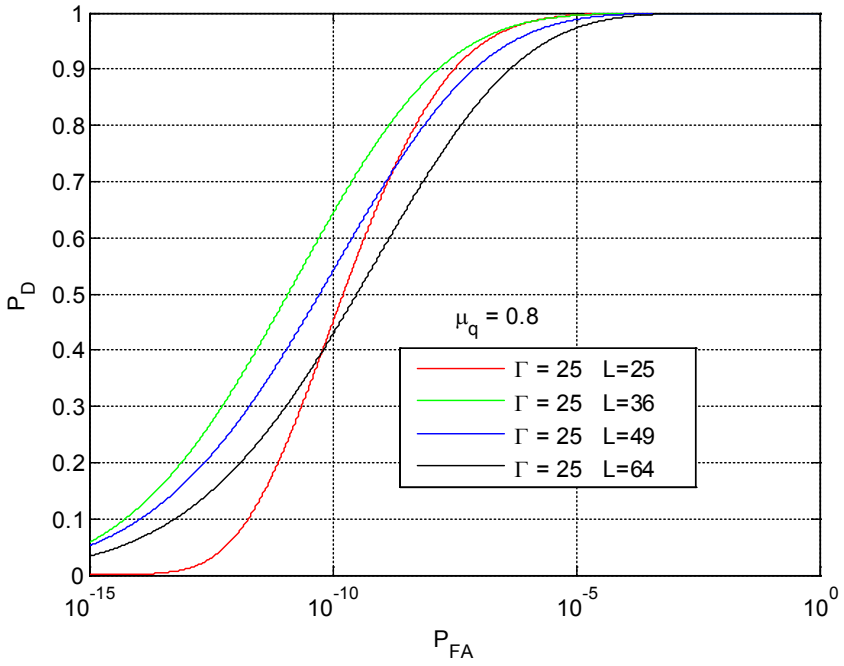

Figure 40: Plot of ROC curve for $\Gamma = 25$ (i.e. $\ell = 25$) for $\mu_q = 0.8$ and varying number of looks, $L = \{25, 36, 49, 64\}$

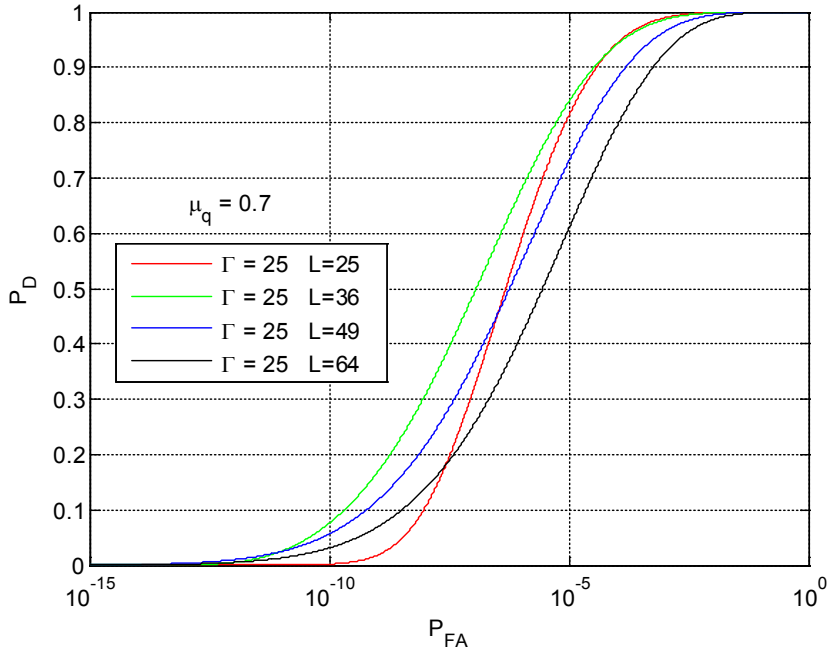

Figure 41: Plot of ROC curve for $\Gamma = 25$ (i.e., $\ell = 25$) for $\mu_q = 0.7$ and varying number of looks, $L = \{25, 36, 49, 64\}$

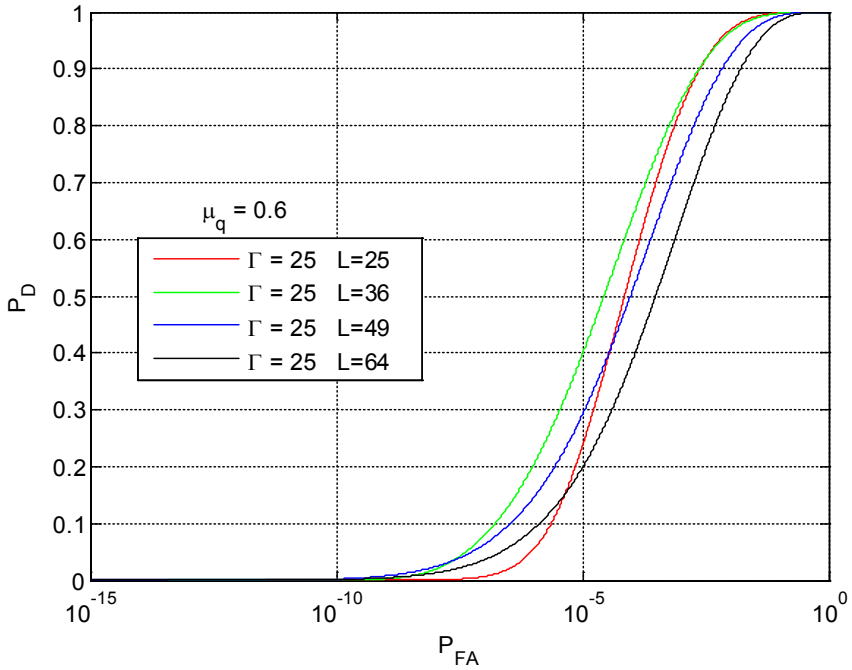

Figure 42: Plot of ROC curve for $\Gamma = 25$ (i.e., $\ell = 25$) for $\mu_q = 0.6$ and varying number of looks, $L = \{25, 36, 49, 64\}$

7. Other considerations

Key concepts in this section: The proposed analytical model is a simplification of the general case, much like Swerling models for radar detection. As in the latter, this model is useful as long as the limitations are considered. Also, as with the Swerling models, this model can be extended to other cases, although we do not do so in this report.

The model developed above gives an analytic method for evaluating the effect of resolution on CCD. There are other considerations in practical detection in CCD.

In the model, false-alarm rates are assumed to be due to the statistical properties of a quiescent background which is assumed to be sampled from a population with a constant coherence. In a practical situation, the population coherence within the CCD image varies due to varying backscatter, shadows, vegetation, radar processing issues, etc. These are likely to be a more prevalent source of false-alarm and need to be handled in some manner.

Another important difference is that in this model we consider detection with only a *single* consistent change region. In a practical CCD images, the "tell" for change is a pattern of multiple resolution cells that have some indication of some specific type of change.

Similarly, in human interpretation of data, the person will perform additional averaging and interpretation that assists in reducing the probability of false-alarm from their perspective. For example, if there is a modest change region in large region of no-change, the human interpreter will naturally average over the no change region well beyond the number of looks used in the multilook window for coherence estimation. In this respect the model presented in this document is limited.

In spite of each of these practical issues, the author argues that the basic model presented above is valuable for system design and operates much as ROC curves are valuable for standard radar detection. In some sense, the discussion in this document is similar to Swerling's models for radar detection.

This page left intentionally blank.

8. Conclusions and Summary

This report has developed a model for the effect of resolution on coherent change detection. This document is intended to support the understanding of coherent change detection (CCD) for radar system designers and allow them to make performance trade-offs.

A few results from this document are summarized here in no order of pre-eminence:

1) Resolution is a key parameter in CCD performance. There are two different resolutions to consider in CCD: 1) the SAR resolution; and 2) the size, or resolution, of the multilook estimation window.
2) CCD is a detection process; therefore, evaluating the the receiver operating characteristic (ROC) curve as a function of resolution is a reasonable measure of the performance.
3) We want as many looks as possible on both change and no-change regions, which means if all else is equal, finer resolution improves CCD performance.
4) It is the size of the change region normalized by the radar resolution that sets the number of independent looks and therefore this sets CCD performance.
5) A limited amount of mixing of the change and no-change within the multilook estimation window where possible does not hurt CCD performance.
6) Only the quiescent coherence, along with the number of looks, influences the probability of false-alarm. It is important for the radar to maintain the background (quiescent) coherence as high as possible, without artificially inflating it.

This page left intentionally blank.

9. References

[ABRA72] M. Abramowitz, and I. Stegun, *Handbook of Mathematical Functions with Formulas, Graphs, and Mathematical Tables*, Courier Dover Publications, 1972.

[BICK14] D. L. Bickel, "SAR Image Effects on Coherence and Coherence Estimation", *SAND2014-0369*, January, 2014.

[BICK15] D. L. Bickel, internal memorandum titled "Preliminary note on receiver operating characteristic curves for CCD", Jan. 2, 2015.

[CART73] G. Carter, et al, "Estimation of the magnitude-squared coherence function via overlapped fast Fourier transform processing", *IEEE Transactions on Audio and Electroacoustics*, Vol. 21, Iss. 4, 1973.

[GUPT00] A. K. Gupta and D. K. Nagar, *Matrix Variate Distributions*, Chapman & Hall/CRC, 2000.

[FISH21] R. A. Fisher, "On the 'Probable Error' of a Coefficient of Correlation Deduced from a Small Sample," *Metron*, vol. 1, no. 5, pp. 3-32, 1921.

[FISH28] R. A. Fisher, "The General Sampling Distribution of the Multiple Correlation Coefficient," *Proceedings of the Royal Society of London. Series A*, vol. 121, no. 788, pp. 654-673, 1928.

[PREI06] M. Preiss, D. A. Gray, N. J. S. Stacy, "Detecting Scene Changes Using Synthetic Aperture Radar Interferometry", IEEE Transactions on Geoscience and Remote Sensing, Vol. 44, No. 8, August 2006.

[SHAN88] K. S. Shanmugan, A. M. Breiphol, *Random Signals: Detection, Estimation, and Data Analysis*, John Wiley & Sons, Inc., 1988.

[SHEP07] K. Sheppard, "Positive Semi-Definite Matrix Multiplicative Error Models", working paper, University of Oxford, June, 2007.

[TAN83] W. Y. Tan and R. P. Gupta, "On approximating a linear combination of central wishart matrices with positive coefficients", *Communications in Statistics - Theory and Methods*, Vol. 12, No. 22, Jan 1,1983.

[TOUZ96] R. Touzi, A. Lopes, "Statistics of the Stokes parameters and of the complex coherence parameters in one-look and multilook speckle fields", IEEE Transactions on Geoscience and Remote Sensing, Vol. 34, Iss. 2, 1996.

[ZEBK92] H. A. Zebker and J. Villasenor, "Decorrelation in interferometric radar echoes," *IEEE Trans. On Geoscience and Remote Sensing*, vol. 30, no. 5, pp. 950–959, Sep. 1992.

This page left intentionally blank.

10. Appendix A: Model for resolution analysis

This appendix contains the math for the model of resolution and coherence presented in this report. The first part of this appendix provides a general discussion of the model. The second part presents the mathematical model for the case where the change region is larger than the multilook area. The third derives the mathematical model when the change region is less than the multilook area.

Note that the key to the analysis of performance in the main body of this report is the receiver operating characteristic (ROC) curves to describe detection as a function of coherences and resolution. Therefore, in this appendix we need to derive the cumulative probability density model.

10.1 General analysis discussion for the model

The analysis in this document is about detection of change in CCD as a function of resolution. In CCD we are interested in the detection of a disturbance that leads to a change in coherence relative to the undisturbed quiescent background. Generally we want to detect this coherence change. To quantify the detection process, we are interested in employing receiver operating characteristic (ROC) curves. These are plots of the probability of detection versus probability of false-alarm for varying parameters. The parameters of interest in this document include the size of the change region, the population coherence of the no-change (quiescent) region, multilook resolution cell size, and Rayleigh resolution cell size.

As a brief review, the ROC curves follow from classic Neyman-Pearson detection theory [SHAN88]. In this detection theory, we make a decision in favor of one hypothesis, H_1, or the other, H_0, based upon our test statistic, $\Lambda(z)$, being greater than, or less than a specific threshold, λ_{th}. This is written as:

$$\Lambda(z) = \frac{p(z|H_1)}{p(z|H_0)} \underset{H_0}{\overset{H_1}{\gtrless}} \lambda_{th} \tag{12}$$

Figure 43 illustrates this detection process.

The probability that we chose H_1 correctly is referred to as the probability of detection. In radar, the main error probability that we are usually interested in is the probability of false-alarm. This is the probability that we chose H_1 given that H_0 has occurred. The ROC curves convey the probability of detection versus false-alarm for varying threshold, and distribution parameters.

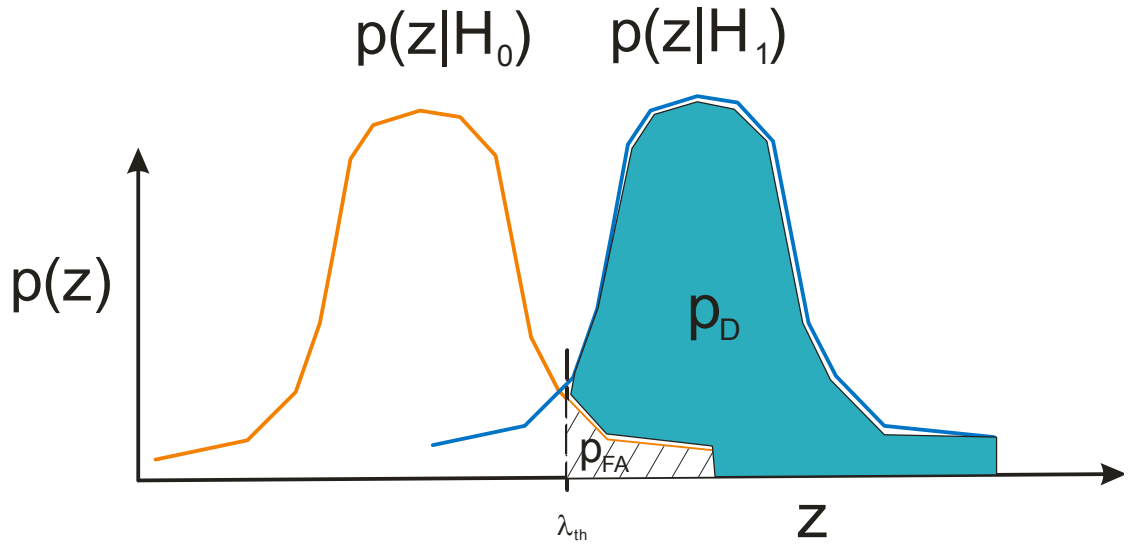

Figure 43: Cartoon illustrating Neyman-Pearson detection for standard radar detection

In CCD, the test statistic is the estimated (sample) coherence, $\hat{\mu}$, over the multilook estimation region. For standard radar detection theory, the distribution parameter information is contained in the signal-to-noise ratio (SNR); however, for the distribution of the CCD test statistic we will be interested in the population coherence[18] and the number of independent looks.

Note that the classic Neyman-Pearson detection problem is transposed for CCD. In typical Neyman-Pearson detection problems, we want to detect objects above some threshold. In CCD, we want to detect the loss of coherence due to a change. The classic detection hypotheses relationship is commuted because we will want to detect coherence below some threshold. In addition, for standard radar ROC curves the signal-to-noise ratio (SNR) is adequate for defining the separation between the hypotheses. In CCD the separation of between hypotheses is a function of both the number of independent looks and the population coherence.

The probabilities are required for generating ROC curves, specifically we need the cumulative distribution function for coherence as a function of the population coherence, the number of independent looks, and the coherence threshold. The development of the probability function for coherence was first done by Fisher in 1921 [FISH21]. A more convenient derivation for us will be the development in terms of the central Wishart distribution for the sample covariance matrix based on bivariate complex circularly Gaussian clutter and noise in [TOUZ96].

[18] Signal-to-noise ratio plays a role in the population coherence but is not the only factor (see [BICK14] and reference therein).

The fundamental parameters in the (complex) central Wishart distribution function are the degrees-of-freedom, ν, and the scale (or diffusion) matrix, $\mathbf{\Sigma}$. The (complex) Wishart distribution of the sample covariance matrix (under the bivariate circularly Gaussian, etc. assumption) then is written as $\mathbf{S} \sim \mathbb{C}W(\nu, \mathbf{\Sigma})$. It becomes obvious that the Wishart distribution is defined by the knowledge of these two parameters. For our zero-mean bivariate case, the scale matrix, $\mathbf{\Sigma}$, is given by[19]:

$$\mathbf{\Sigma} = \begin{bmatrix} \sigma_1^2 & \mu\sigma_1\sigma_2 \\ \mu^*\sigma_1\sigma_2 & \sigma_2^2 \end{bmatrix} \tag{13}$$

From the development in [TOUZ96], if the covariance matrix follows the central Wishart distribution, then the probability density function of the (sample) coherence follows directly from knowledge of parameters of this Wishart distribution. In particular, if we know ν and μ (the population coherence) in equation (13) for the Wishart distribution then we can use the equation in [TOUZ96] to yield the probability distribution of the sample coherence.

The original solution for the cumulative distribution with ν an integer was presented in [FISH28]. We will use the version from [CART73] in this document.

Generally, we will assume that the change region area has a population coherence of zero, designated as $\mu_c = 0$. We will assume that the no change, or quiescent area has a population coherence of μ_q, which is between 0 and 1.

10.2 The proposed model

We have seen from the previous section that the fundamental parameters for detection in CCD are the degrees-of-freedom, ν, and the population coherence, μ, from the scale matrix $\mathbf{\Sigma}$. For the purposes of the report then, we need to understand the behavior of these parameters as a function of size of the change region relative to the resolution size.

In coherent change detection (CCD), there are actually two different resolutions of interest. The first resolution is the synthetic aperture radar (SAR) Rayleigh resolution. This is the resolution that normally comes to mind. The second resolution is the size of the averaging area used to estimate the coherence, which is related to the number of looks. Note that resolution is typically thought of as a linear measure; however, in CCD it is the resolution area that is important. Figure 44 illustrates the two different resolutions.

The size of the change region with respect to these resolution areas will be a key variable. A simple thought experiment says that the more samples we can observe that have

[19] Note that the scale matrix is also the true covariance matrix in this case.

changed (and that have not changed), the better detection decision we will be able to make, so this makes intuitive sense. Without loss of generality in this model, we can normalize all resolution area measures relative to a single SAR Rayleigh resolution cell area. In addition, we will assume that the change area is relatively small with respect to the non-change area.

Based upon this discussion, we have decided to simplify the analysis by separating our model into two general cases. The first case assumes that the region of change at least covers an entire multilook resolution area. In fact we will assume that it is exactly one multilook resolution size. The second case is where the change area covers less than a multilook resolution area. This second case also includes the case where the change area is less than a radar Rayleigh resolution area. The reason for this differentiation will become apparent from discussion later in this appendix.

The terminology used in this appendix includes the SAR Rayleigh resolution cell (area) which is designated ρ_R and which we normalize to $\rho_R = 1$ without loss of generality. The multilook (CCD estimation "box") size is then designated $\rho_{ml} = L\rho_R = L$. We also designate the change region area as Γ_c, which when normalized by ρ_R (i.e., we normalize to $\rho_R = 1$) is written as $\Gamma = \Gamma_c / \rho_R$. The model is then split into $\Gamma \geq L$ (again, we really consider $\Gamma = L$) or $\Gamma < L$. To be even more specific, for our analysis we will be really be partitioning the cases into change regions that cover the *whole* multilook resolution cell, versus change regions that cover a partial multilook resolution cell. Included in the latter is the case where the change covers a partial Rayleigh resolution cell. Therefore, although we will generally not consider it in our analysis, the shape of Γ_c, as well as the area it covers, will be important. Figure 45 shows the two cases for the regions of change that we consider in this appendix. We will proceed under this understanding.

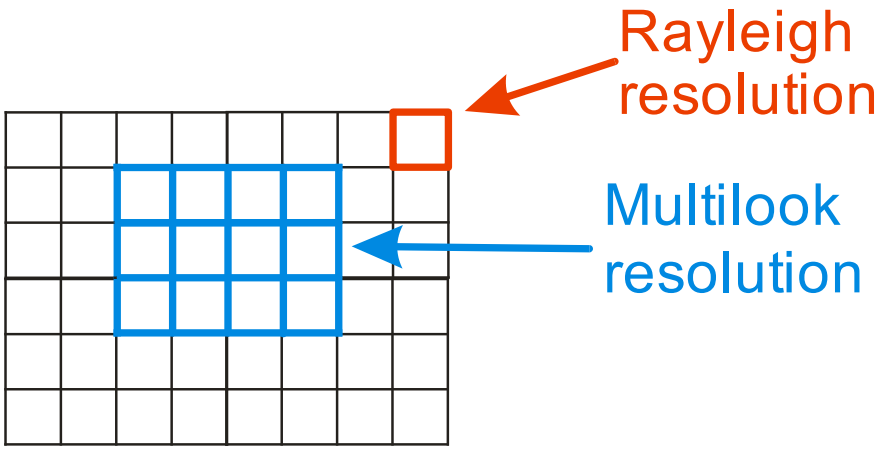

Figure 44: Illustration of two resolutions in CCD in terms of image pixels

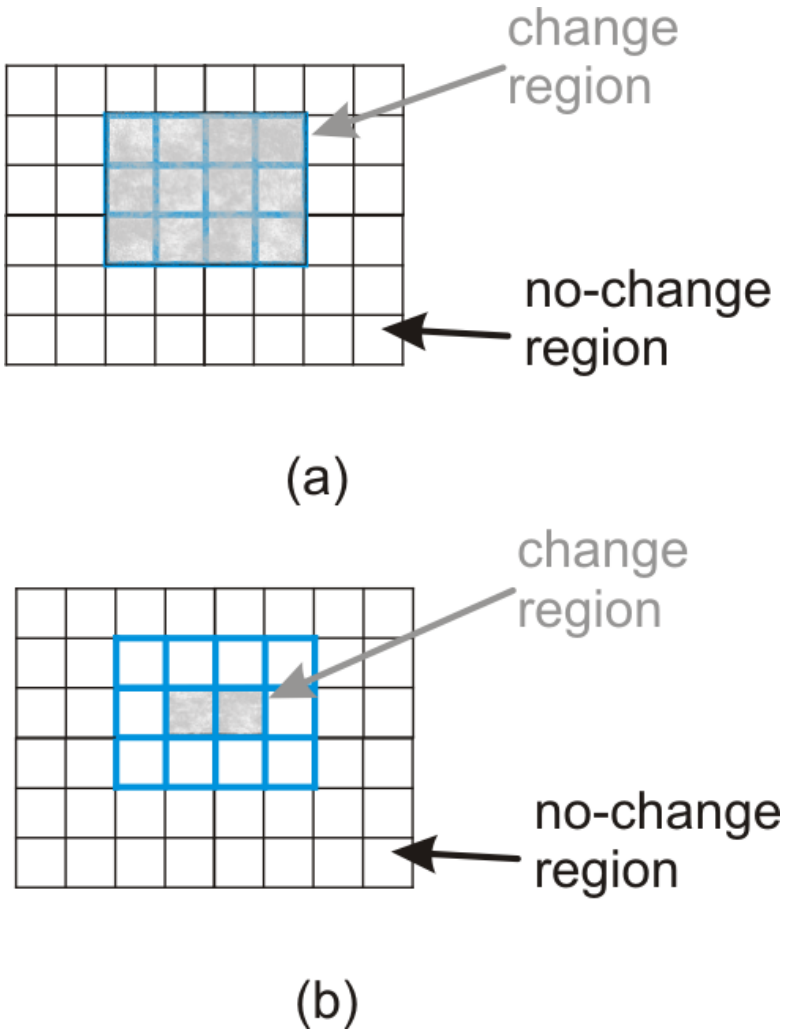

Figure 45: Two different change region cases (a) change covers an entire multilook resolution cell; (b) change covers a partial multilook resolution cell

It is *important to note* that regardless of the change region case being considered above for a given threshold *the probability of false-alarm does not change* since we always assume a large quiescent region. However, the probability of detection does change between the different cases because we dilute the change region when the change region is smaller than a multilook resolution cell size.

Before proceeding on to the discussion of the different change regions, we want to note that the key to the mathematical development in this document is that regardless of the resolution case, we will assume that the sample covariance matrix can be adequately approximated as a central Wishart distribution. From the discussion above this means it suffices to generate the degrees-of-freedom ν, and the scale matrix, $\mathbf{\Sigma}$ for each of the three resolution cases. We now present this development.

10.3 Change region at least as large as the multilook resolution cell

A very good reference for the discussion in this section is given in [PREI06]. Independently, but belatedly, very similar work was done in [BICK15], including very similar conclusions. The work in [PREI06] is nicely done and is a recommended read by this author; however, for convenience we will follow [BICK15] in this section.

For the case where the change region is as large as the multilook resolution cell, the Wishart distribution and the relation to the sample coherence was explained in [TOUZ96]. Therefore, it remains for us to use those results to develop the ROC curves.In this case, since the change regions cover the entire multilook estimation window we can think of the CCD as detection of a no coherence area against the background quiescent coherence. For the ROC curves the probability of detection is the probability that the estimated coherence is less than a given threshold i.e.:

$$P_D = P\left(\hat{\mu} \le \lambda_{th} \middle| \mu_c = 0, L\right) \tag{14}$$

where P_D is the probability of detection, $\hat{\mu}$ is the estimated (sample) coherence, as stated above μ_c is the population coherence (assumed to be zero in the change region), and L is the number of independent looks[20]. The probability of a false-alarm is the probability that the estimated background coherence is less than this threshold, i.e.:

$$P_{FA} = P\left(\hat{\mu} \le \lambda_{th} \middle| \mu_q, L\right) \tag{15}$$

where P_{FA} is the probability of detection, as stated above μ_q is the population coherence of the no-change quiescent region.

From [TOUZ96], the probability density function of the coherence is in general:

$$p\left(\hat{\mu} \middle| \mu, L\right) = 2\left(L-1\right)\left(1-\mu^2\right)^L \hat{\mu}\left(1-\hat{\mu}^2\right)^{(L-2)} {}_2F_1\left(L, L; 1; \hat{\mu}^2\mu^2\right) \tag{16}$$

where $\hat{\mu}$ is the sample coherence, and μ is the generic population coherence. One of the assumptions in the above equation is that the population coherence is stationary across the estimation multilook area.

For the ROC curve calculations we need the cumulative distribution, which is given in [CART73] for integer L as:

[20] Note that in the Wishart distribution, the number of degrees-of-freedom, ν, becomes the number of independent looks, L.

$$P\left(\hat{\mu} < \lambda_{th} \middle| \mu, L\right) = \lambda_{th}^2 \left(\frac{1-\mu^2}{1-\mu^2\lambda_{th}^2}\right)^L \sum_{k=0}^{L-2} \left(\frac{1-\mu^2}{1-\mu^2\lambda_{th}^2}\right)^k {}_2F_1\left(-k, 1-L; 1; \mu^2\lambda_{th}^2\right) \tag{17}$$

Plugging $\mu_c = 0$ into equation (17), the probability of detection can be shown to lead to a nice and simple result of:

$$P_D = 1 - \left(1 - \lambda_{th}^2\right)^{L-1} \tag{18}$$

The P_{FA} is more complicated and follows:

$$P_{FA} = \lambda_{th}^2 \left(1-\mu^2\right)^L \sum_{k=0}^{L-2} \left[\left(1-\lambda_{th}^2\right)^k {}_2F_1\left(k+1, L, 1; \lambda_{th}^2\mu^2\right)\right] \tag{19}$$

As shown in Appendix C, the particular form we have chosen for equation (19) was modified from [CART73] for convenience because it can be shown to have a nice recursive form.

If we are given a desired probability of detection, we can solve for the threshold using equation (18):

$$\lambda_{th} = \sqrt{1 - \left(1 - P_D\right)^{1/(L-1)}} \tag{20}$$

It is typically more desirable to set the threshold to yield a specific probability of false-alarm. Unfortunately equation (19) is a transcendental equation that does not lend itself to simple inversion solution for the threshold. We address this in the main text of this document.

Given all of the above information, we now have the all the tools we need to perform the ROC curve plots for this case.

10.4 Change region at less than the multilook resolution cell

As discussed in the main body of this report, when the change region is contained within multilook resolution cell size and is smaller than the multilook resolution cell size, we mix two distributions with different statistics. This violates the stationarity assumption used in the standard derivations of the sample coherence from [TOUZ96]. In general, this particular mixing of distributions is typically messy and may not be tractable [SHEP07]. There is a nice approximation that is used and that we will take advantage of in this document. The approximation was first proposed in [TAN83] but we follow the development in [GUPT00].

The key to the approximation is the assumption that the linear combination of the central Wishart distributions can be approximated as a different central Wishart distribution. This approximation only covers central Wishart distributions. At first blush, this does not help us because the Wishart distribution is for the sample covariance matrix and not the distribution for the sample coherence. However, if one recognizes that the development of the sample coherence distribution [TOUZ96] starts with the central Wishart and in the end only requires the knowledge of parameters of the central Wishart distribution, the solution becomes simple[21]. We just need to find the parameters of the central Wishart used to approximate the linear combination of the distributions. Those parameters can be plugged into the distribution of the sample coherence.

We now discuss the derivation of these parameters. In some respects we are trying to "fit" the resulting linear combination of central Wishart distributions to a new central Wishart distribution. As mentioned previously, the parameters required for the fitted central Wishart distribution are the degrees-of-freedom and the scale matrix.

Tan, et al, proposed that an approximation developed originally for univariate random variables could be extended to the multivariate case [TAN83]. The univariate approximation technique is referred to as Satterthwaite's approximation. It establishes the necessary distribution parameters by setting the first two moments of the linearly combined distributions to the new approximating distributions moments. The extension to the multivariate case is sometimes referred to at the multivariate Satterthwaite approximation.

A difficulty that arises in the multivariate case is that the number of variables available for the fit can exceed the number necessary to define the approximating distribution. Tan, et al, resolve this by using the mean and Wilks' generalized variance for the multivariate case in the place of the first two moments in the univariate case. Setting the mean and generalized variance of the linear combination of the distribution components to those of the approximating central Wishart distribution allows us to solve for the degrees-of-freedom and the scale matrix of the approximating distribution.

We now present the application of this approximation to our problem. Detailed derivation of the estimation of the approximating distribution degrees-of-freedom and the scale matrix are presented in Appendix C. Given these parameters, we show how it applies to our problem of coherence distribution with mixed coherence within the multiook resolution cell.

In order to address the case of the change region size being less than the multilook resolution area, we must address a challenge of relaxing the assumption used in the previous section where the population coherence is stationary across the estimation multilook area. In general in mathematics, this problem is known to be quite challenging, if not analyitically unrealizable. However, we extend the use of the above approximation to the realm of SAR coherence. This result represents a new contribution to the field.

[21] We foreshadowed this in the discussion of the complex central Wishart distribution above.

We point out issues with the approximation in the main body of the report; however, we note that in general it does provide us with a framework for assessing resolution and CCD.

For this appendix, we will assume that:

$$\Sigma_1 = \sigma^2 \begin{bmatrix} 1 & \mu_q \\ \mu_q & 1 \end{bmatrix} \tag{21}$$

and

$$\Sigma_2 = \sigma^2 \begin{bmatrix} 1 & 0 \\ 0 & 1 \end{bmatrix} \tag{22}$$

where we assume σ^2 is the mean power in the clutter plus noise for all pixels (resolution cells).

Using ν_1 independent samples from a population with covariance matrix, Σ_1, to estimate a sample covariance matrix, S_1, leads to a central Wishart distribution $S_1 \sim W(\nu_1, \Sigma_1)$. Likewise, the estimate of the sample covariance matrix of S_2 using ν_2 independent samples from a population with covariance matrix, Σ_2, has a central Wishart distribution of $S_2 \sim W(\nu_2, \Sigma_2)$.

Now assume that we are estimating the covariance matrix of S, where the estimate window (multilook resolution) contains samples $\nu_s = \nu_1 + \nu_2$, of which ν_1 are from the population Σ_1 and ν_2 are from the population Σ_2. The resulting estimate of the covariance matrix, S, is a mixture of the two populations, $S \sim S_1 + S_2$. From Appendix C, the distribution is approximately $S \sim W(\nu, \Sigma)$ where:

$$\nu \approx \nu_s \frac{\left[1 - \left(\frac{\nu_1}{\nu_s}\right)^2 \mu_q^2\right]}{\left(1 - \frac{\nu_1}{\nu_s}\mu_q^2\right)\left[1 + 4\left(\frac{\nu_1}{\nu_s}\right)\mu_q^2 \frac{\left(1 - \frac{\nu_1}{\nu_s}\right)}{\left(1 - \frac{\nu_1}{\nu_s}\mu_q^2\right)^2}\right]^{1/3}} \tag{41}$$

and:

$$\Sigma = \frac{\nu_s}{\nu}\sigma^2 \begin{bmatrix} 1 & \frac{\nu_1}{\nu_s}\mu_q \\ \frac{\nu_1}{\nu_s}\mu_q & 1 \end{bmatrix} \tag{36}$$

One of the key contributions in this document is the recognition that based upon this approximation, we can use equation (16) from above as an estimate of the probability density function of the resulting sample coherence where we set $L = \nu$ and $\mu = (\nu_1/\nu_s)\mu_q$. Notice that one of the results of this approximation is that the population coherence within this mixed region is a simple linear weighting of the coherences contained within the estimation window. We restate this result in the following equation in order to be able to reference it later:

$$\mu_c = \frac{\nu_1}{\nu_s}\mu_q \tag{36}$$

Using the above results, the resulting (approximate) probability density function is:

$$p\left(\hat{\mu}\middle|(\nu_1/\nu_s)\mu_q,\nu\right) = 2(\nu-1)\left(1-\frac{\nu_1^2}{\nu_s^2}\mu_q^2\right)^{\nu}\hat{\mu}\left(1-\hat{\mu}^2\right)^{(\nu-2)}{}_2F_1\left(\nu,\nu;1;\hat{\mu}^2\frac{\nu_1^2}{\nu_s^2}\mu_q^2\right) \tag{23}$$

for $\nu > 3$. This equation works because it is known that non-integer values of are ν valid. Unfortunately, the equation for the cumulative distribution of the sample coherence requires integer values of ν . The estimate of the cumulative distribution in the non-integer case can be obtained either through numerical integration of equation (23) or by interpolation of equation (17) from nearby integer values. In either case, it is *important to note* that for a given threshold the probability of false-alarm does not change in the model since we assume a large quiescent region; however, the probability of detection does change because we have diluted the change region.

11. Appendix B: Another method of fitting

In the previous appendix, we a developed a model based upon [TAN83] and showed how it could be used to generate an approximation to sample coherence when there is a mixture of two different population coherence statistics in the coherence estimation region. The method presented above can crudely be thought of as "fitting" the mixed distribution to a central Wishart distribution. This "fitting" has a solid mathematical heritage and basis from the Satterthwaite's work with univariate random variables. In this section, we present another fit that is more heuristic, and in a sense, brute force.

Note that in the Satterthwaite multivariate approximation, we needed to boil the number of free variables down in the covariance matrix to a single variable to avoid an overdetermined "fit" to the complex Wishart distribution. In the Satterthwaite approximation, the generalized variance is used. As will now be discussed, in this appendix we will propose the estimated coherence as that variable.

As with the preceding model, the basis for the model in this section is the assumption that the covariance of the mixed distribution is approximated by a complex central Wishart distribution. The resulting coherence probability distribution under this condition is known and given in equation (16). The heuristic model used here maintains the assumed population coherence (i.e., the scale matrix) from Tan's method given in equation (36). The difference is that we estimate the degrees-of-freedom by matching the variances[22] of simulated data to the probability density function given in equation (16).

In Tan's method, the covariance means and the generalized variance are matched to the approximating distribution. The matching of the means led essentially to the weighted population coherence, which we will maintain in this method. The generalized variance led to the number of degrees-of-freedom. We will expound briefly on the meaning of the generalized variance in this section. Although this discussion can be shown in a general case, we only need concern ourselves with the bivariate case.

It is well known that contours of constant probability for a bivariate Gaussian distribution are an ellipse. What is less well known is that the generalized variance is a measure of the square of the area (volume, in general) of the ellipse (ellipsoid, in general). Therefore, the generalized variance is a metric for the spread of the distribution. Tan's method chooses the degrees of freedom to match the spread of the linearly combined distributions with that of the spread of the approximating distribution.

In the bivariate case, there is a relationship between the population coherence and the population generalized variance. Therefore, this proposed heuristic method is a different way to fit to the spread of the distribution, which is assumed to be a complex central Wishart.

[22] Note that the standard distribution for estimated coherence there is a correspondence between the variance and the mean, so theoretically either could be chosen *if the central Wishart distribution approximation holds*.

This page left intentionally blank.

12. Appendix C: Collection of supporting analysis

This appendix provides the math for supporting discussion in this document.

11.1 Recursive calculation of cumulative coherence distribution

The cumulative distribution for the coherence was presented in equation (17) and is repeated here from [CART73]:

$$P\left(\hat{\mu} < \lambda_{th} \middle| \mu, L\right) = \lambda_{th}^2 \left(\frac{1-\mu^2}{1-\mu^2\lambda_{th}^2}\right)^L \sum_{k=0}^{L-2} \left(\frac{1-\mu^2}{1-\mu^2\lambda_{th}^2}\right)^k {}_2F_1\left(-k, 1-L; 1; \mu^2\lambda_{th}^2\right) \tag{17}$$

We use various equations from [ABRA72] to rewrite the above equation in a recursive form.

First, using [ABRA72] the hypergeometric term in the equation above can be written as;

$${}_2F_1\left(-k, 1-L; 1; \lambda_{th}^2\mu^2\right) = \left(1-\lambda_{th}^2\mu^2\right)^{L+k} {}_2F_1\left(k+1, L, 1; \lambda_{th}^2\mu^2\right) \tag{24}$$

resulting in:

$$P\left(\hat{\mu} < \lambda_{th} \middle| \mu, L\right) = \lambda_{th}^2 \left(1-\mu^2\right)^L \sum_{k=0}^{L-2} \left[\left(1-\lambda_{th}^2\right)^k {}_2F_1\left(k+1, L, 1; \lambda_{th}^2\mu^2\right)\right] \tag{25}$$

The following recursive relationship can be used to advantage:

$$\begin{aligned} k\left(1-\lambda_{th}^2\mu^2\right) {}_2F_1\left(k+1, L; 1; \lambda_{th}^2\mu^2\right) &= \left[2k-1-\left(k+L\right)\lambda_{th}^2\mu^2\right] {}_2F_1\left(k, L, 1; \lambda_{th}^2\mu^2\right) \\ &+\left(1-k\right) {}_2F_1\left(k-1, L; 1; \lambda_{th}^2\mu^2\right) \end{aligned} \tag{26}$$

recalling that:

$${}_2F_1\left(0, L; 1; \lambda_{th}^2\mu^2\right) = 1 \tag{27}$$

Therefore, each k^{th} term within the brackets of the sum in equation (25), starting with $k = 0$, incrementally can be generated in a simple recursive manner making for an elegant calculation of the cumulative distribution for coherence.

11.2 Application of the Satterthwaite approximation

In this section we present the form of the Satterthwaite approximation that we use in this document. As mentioned above the discussion of the approximation initially was proposed by [TAN83] but we will follow the development in [GUPT00].

Given a random variable, S_i, with central Wishart probability distribution designated as $S_i \sim W(\nu_i, \Sigma_i)$ where ν_i is the degrees-of-freedom and Σ_i is the scale matrix, the mean is known to be:

$$E(S_i) = \nu_i \Sigma_i \tag{28}$$

Given a mixture of two independent central Wishart distributed random variables, S_1 and S_2, if $\Sigma_1 = \Sigma_2 = \Sigma$, then the mean of the sum of the two random variables is:

$$E(S) = E(S_1 + S_2) = \nu\Sigma = (\nu_1 + \nu_2)\Sigma \Rightarrow \nu = (\nu_1 + \nu_2) \tag{29}$$

which is a fundamental property of the Wishart distribution.

The Satterthwaite approximation [TAN83] approximates the linear combination of central Wishart distributions as a central Wishart distribution. To establish the approximating distribution, we need to find the appropriate values of the degrees-of-freedom and the scale matrix . This involves two parts. The first part of the approximation is to set the mean of the linear combination of the random variables to the mean of the approximating distribution. In our case of interest we are considering the linear combination of two central Wishart distributions that we designate as $S_1 \sim W(\nu_1, \Sigma_1)$ and $S_2 \sim W(\nu_2, \Sigma_2)$. The linear combination that we are concerned with is:

$$S \sim S_1 + S_2 \tag{30}$$

In the approximation case we assume that even if $\Sigma_1 \neq \Sigma_2$ we can approximate the mean of the random variable in equation (30) as:

$$\nu\Sigma \approx \nu_1\Sigma_1 + \nu_2\Sigma_2 \tag{31}$$

The scale matrix for the approximating central Wishart distribution is one of the two parameters that we need[23]. Using equation (31), we have that the scale matrix of the approximating distribution is:

$$\Sigma \approx \frac{\nu_1\Sigma_1 + \nu_2\Sigma_2}{\nu} \tag{32}$$

[23] We note that equation (34) contains the other parameter we need, ν, therefore we do not really have the scale matrix even yet.

For this appendix, we will assume that:

$$\Sigma_1 = \sigma^2 \begin{bmatrix} 1 & \mu_q \\ \mu_q & 1 \end{bmatrix} \tag{33}$$

and

$$\Sigma_2 = \sigma^2 \begin{bmatrix} 1 & 0 \\ 0 & 1 \end{bmatrix} \tag{34}$$

In the preceding appendix, we discuss the above choice of these individual scale matrices.

To simplify, let:

$$\nu_s = \left(\nu_1 + \nu_2\right) \tag{35}$$

then equation (32) becomes:

$$\Sigma = \frac{\nu_s}{\nu}\sigma^2 \begin{bmatrix} 1 & \frac{\nu_1}{\nu_s}\mu_1 \\ \frac{\nu_1}{\nu_s}\mu_1 & 1 \end{bmatrix} \tag{36}$$

Next we need to solve for the degrees-of-freedom, ν. This is done by equating the generalized variance of the approximating distribution to that of the linear combination of the random variables, $\left|\mathrm{v}_\sigma\right|$. The work in [TAN83] and [GUPT00] is a bit involved, so we will just hit the highlights.

Equating the generalized variances for our case yields:

$$\left|\sum_{i=1}^{2} \nu_i K_r^- \left(\Sigma_i \otimes \Sigma_i\right) K_r\right| = \left|\nu K_r^- \left(\Sigma \otimes \Sigma\right) K_r\right| \tag{37}$$

where K_r is an elimination matrix, and $\otimes$ means take the Kronecker product.

After a healthy dose of algebra and matrix theorems, for our bivariate case the solution for the degrees-of-freedom becomes:

$$\nu \approx \frac{\left|\nu\Sigma\right|}{\left|\mathrm{v}_\sigma\right|^{1/3}} \tag{38}$$

where:

$$\left|\nu\Sigma\right| = \nu_s^2\sigma^4\left[1-\left(\frac{\nu_1}{\nu_s}\right)^2\mu_1^2\right] \tag{39}$$

and where the following can be shown:

$$\left|\mathrm{v}_\sigma\right| = \sigma^{12}\nu_s^3\left[1-\left(\frac{\nu_1}{\nu_s}\right)\mu_1^2-\left(\frac{\nu_1}{\nu_s}\right)^2\mu_1^2\left(4+\mu_1^2\right)+\left(\frac{\nu_1}{\nu_s}\right)^3\mu_1^4\left(4-\mu_1^2\right)\right] \tag{40}$$

The result is that:

$$\nu \approx \nu_s \frac{\left[1-\left(\frac{\nu_1}{\nu_s}\right)^2\mu_1^2\right]}{\left(1-\frac{\nu_1}{\nu_s}\mu_1^2\right)\left[1+4\left(\frac{\nu_1}{\nu_s}\right)\mu_1^2\frac{\left(1-\frac{\nu_1}{\nu_s}\right)}{\left(1-\frac{\nu_1}{\nu_s}\mu_1^2\right)^2}\right]^{1/3}} \tag{41}$$

As a quick check of equation (41), if $\mu_1 = 0$, we arrive at $\nu \approx \nu_s$, which is what we would expect from the Wishart property that we discussed above.

So finally, the approximating distribution for S in equation (30) is:

$$S \sim W\left(\nu,\Sigma\right) \tag{42}$$

where ν is in equation (41) and Σ is in equation (36).

q.e.d.

12.3 Application of the Satterthwaite approximation with correlation in Σ_2

In the previous derivation we assumed that the second Wishart distribution had a scale matrix of the form in equation (34). What if it were of the following form:

$$\Sigma_2 = \sigma^2\begin{bmatrix}1 & \mu_2\\ \mu_2 & 1\end{bmatrix} \tag{43}$$

where $\mu_2 \neq 0$? In this case, the approximation scale matrix becomes:

$$\Sigma = \frac{\nu_s}{\nu}\sigma^2 \begin{bmatrix} 1 & \dfrac{(\nu_1\mu_1 + \nu_2\mu_2)}{\nu_s} \\ \dfrac{(\nu_1\mu_1 + \nu_2\mu_2)}{\nu_s} & 1 \end{bmatrix} \tag{44}$$

which reduces to equation (36) in the previous subsection when $\mu_2 = 0$.

The degrees-of-freedom parameter is more complicated in this case but can be derived following the same procedure as above. We will not present the full equation here to save space, although we briefly show a step towards the solution of equation (38) for this case. We can readily find that:

$$\nu \approx \nu_s \frac{\left[1 - \dfrac{(\nu_1\mu_1 + \nu_2\mu_2)^2}{\nu_s^2}\right]}{\left|\begin{bmatrix} 1 & 2\mu_2 + 2\left(\dfrac{\nu_1}{\nu_s}\right)(\mu_1 - \mu_2) & \mu_2^2 + \left(\dfrac{\nu_1}{\nu_s}\right)(\mu_1^2 - \mu_2^2) \\ \mu_2 + \left(\dfrac{\nu_1}{\nu_s}\right)(\mu_1 - \mu_2) & 1 + \mu_2^2 + \left(\dfrac{\nu_1}{\nu_s}\right)(\mu_1^2 - \mu_2^2) & \mu_2 + \left(\dfrac{\nu_1}{\nu_s}\right)(\mu_1 - \mu_2) \\ \mu_2^2 + \left(\dfrac{\nu_1}{\nu_s}\right)(\mu_1^2 - \mu_2^2) & 2\mu_2 + 2\left(\dfrac{\nu_1}{\nu_s}\right)(\mu_1 - \mu_2) & 1 \end{bmatrix}\right|^{1/3}} \tag{45}$$

This page left intentionally blank.

13. Appendix D: Symbols and terminology

Variable definitions

$\mathbb{C}W$ - is complex Wishart distribution

K_r - is elimination matrix

k - is the integer number of radar resolutions cells within ρ_{ml} where no-change is mixed in with change where $k = L - \ell$. (Also, k is sometimes arbitrary parameter used in various summations)

ℓ - is the integer number of radar resolutions cells within ρ_{ml} where change occurs when we make this assumption, i.e., to simplify analysis we may assume that $\Gamma = \ell$ is an integer, and $1 \le \ell < L$

L - independent looks averaged to estimate the coherence and sets the probability density function (related to ν)

P_D - probability of detection

P_{FA} - probability of false-alarm

S - is a random variable from a sample covariance matrix pulled from a(n approximating) complex central Wishart random variable

S_i - is a random variable from the i^{th} sample covariance matrix pulled from a (true) complex central Wishart random variable

snr - signal-to-noise ratio, assumed equal between images (unitless)

W - is Wishart distribution

Γ_c -, is the area where change occurs

$\Gamma = \Gamma_c / \rho_R$ -is the area where change occurs normalized by (i.e., relative to) the radar resolution

λ_{th} - Neyman-Pearson threshold

μ - the value of the population coherence

$\hat{\mu}$ - the estimate of the coherence (often used to mean the magnitude of this quantity) $\mathbb{C}W(\nu, \boldsymbol{\Sigma})$ - complex central Wishart distribution with degrees-of-freedom, ν , and scale matrix, Σ

μ_c - population coherence of the change region

μ_q - population coherence of the quiescent (no-change) region

ν - is the degrees-of-freedom for Wishart/coherence probability

ν_i - is the degrees-of-freedom for Wishart/coherence probability for the i^{th} region

$\nu_s = \nu_1 + \nu_2$ - is the sum of the degrees-of-freedom for two regions (1 and 2)

ρ_R - "resolution" of the radar, i.e., the Rayleigh resolution (an area in this document)

ρ_{ml} - "multilook resolution" of the radar, i.e., the contiguous area used in a single estimate of a coherence (in this document $\rho_{ml} = L\rho_R$)

Σ -is the scale, or diffusion, matrix for Wishart distribution

Σ_i -is the scale, or diffusion, matrix for the i^{th} Wishart distribution

${}_2F_1(a,b;c;d)$ - the Gauss hypergeometric function

$|\mathbf{X}|$ - determinant of matrix $\mathbf{X}$

$\otimes$ - is the Kronecker product

Terminology

Since the terminology is somewhat unique in this report, and is important to be clear we repeat some of this terminology here.

"change region" – is the region which contains change. The population coherence in this region is designated as μ_c

"multilook resolution" – the size of the area used to estimate the coherence, ρ_{ml}, in this report this $\rho_{ml} = L\rho_R$

"number of looks" – number of independent samples used to estimate the coherence, L

"population coherence" – true (mean) coherence of the region of interest, i.e., the mean coherence we would observe with infinite number of looks, μ

"quiescent region" – is the region which has no change. The population coherence in this region is designated as μ_q

"radar (or Rayleigh) resolution" – the size of the raw resolution cell size for the radar, ρ_R, (note this is really an area in this report). This is set by radar bandwidths in slow and fast-time

"sample coherence" – estimated coherence, $\hat{\mu}$, using L looks

14. Distribution

Unlimited Release

1	MS 0509	A. J. Medina	5300	(electronic copy)
1	MS 0519	D. L. Bickel	5344	(electronic copy)
1	MS 0519	A. Martinez	5344	(electronic copy)
1	MS 0519	R. M. Naething	5344	(electronic copy)
1	MS 0519	A. M. Raynal	5344	(electronic copy)
1	MS 0519	K. R. Czuchlewski	5346	(electronic copy)
1	MS 0519	R. D. West	5346	(electronic copy)
1	MS 0519	J. A. Ruffner	5349	(electronic copy)
1	MS 0519	A. W. Doerry	5349	(electronic copy)
1	MS 0519	L. M. Klein	5349	(electronic copy)
1	MS 0519	R. C. Ormesher	5354	(electronic copy)
1	MS 0532	S. P. Castillo	5340	(electronic copy)
1	MS 0532	B. L. Burns	5340	(electronic copy)
1	MS 0532	W. H. Hensley	5344	(electronic copy)
1	MS 0532	E. D. Gentry	5344	(electronic copy)
1	MS 0532	C. Musgrove	5344	(electronic copy)
1	MS 0532	M. C. Chang	5348	(electronic copy)
1	MS 0532	D. M. Small	5348	(electronic copy)
1	MS 0532	M. E. Thompson	5348	(electronic copy)
1	MS 0533	S. Gardner	5342	(electronic copy)
1	MS 0533	T. P. Bielek	5342	(electronic copy)
1	MS 0533	D. Harmony	5342	(electronic copy)
1	MS 0533	J. A. Hollowell	5342	(electronic copy)
1	MS 0533	R. Riley	5342	(electronic copy)
1	MS 0533	B. G. Rush	5342	(electronic copy)
1	MS 0533	D. G. Thompson	5342	(electronic copy)
1	MS 0533	K. W. Sorensen	5345	(electronic copy)
1	MS 0533	D. F. Dubbert	5345	(electronic copy)
1	MS 0899	Technical Library	9536	(electronic copy)
1	MS 1202	J. G. Chow	5349	(electronic copy)


Sandia National Laboratories